EFFECTS OF LAYER BOUNDARIES ON FWAL AND DIP ESTIMATION (OBLIQUE EVENTS)

by

Benoit Paternoster and Marc Larrère

Earth Resources Laboratory
Department of Earth, Atmospheric, and Planetary Sciences
Massachusetts Institute of Technology
Cambridge, MA 02139

ABSTRACT

Data recorded by the full waveform acoustic logging tool EVA shows events generated at acoustic layer boundaries. These can be interpreted as reflections on and transmissions through interfaces. Ray modelling shows that these events are very sensitive to the dip. After processing of an iso-offset section designed to enhance and separate such events, two sections are interpreted and the dip angles of the interfaces are estimated.

INTRODUCTION

In September 1983, recordings were made in the Burch well in Michigan using the full waveform acoustic logging tool EVA of the Société Nationale Elf Aquitaine (Production). EVA is composed of 5 transmitters at the top spaced 25 cm apart. Twelve receivers are located below the transmitters, each separated by 1 meter. The uppermost receiver is 1 meter below the lowest transmitter. This original geometry achieves spacings between transmitter and receiver that range from 1 meter to 13 meters. The sources are fired in sequences of increasing spacing values. Shoots are triggered every 150 ms. The tool was run at the very slow speed of 6 ft per minute with only 12 combinations of transmitter and receiver, yielding a particularly dense spatial sampling of the formation. A convenient way to display the recorded data is to plot sections of the traces obtained by only one combination of transmitter and receiver versus depth (see Figure 1). These iso-offset sections may be qualitatively read as conventional logs showing the various arrivals, headwaves (P and S)and guided waves (pseudo-Raleigh and Stoneley), with their relative velocities and amplitudes. In addition, the records show rather unusual events: waves are scattered at the interfaces propagating with nearly constant apparent velocities. Since they cut across the usual arrivals at an angle, these waves will be referred to as oblique arrivals. Figure 2 shows some examples from the Burch well. Such arrivals have been observed at other sites, (Koerperich, 1978; Serra, 1984). They are related to bed boundaries or other discontinuities intersecting the borehole. In this paper we study these events using ray theory.

An important aspect of these waves is that a P wave incident upon the interface has generated both P and S transmitted and reflected waves. Such a

conversion cannot take place at a smooth boundary normal to the borehole. One explanation is that P to S conversion takes place because of the dip of the interface. The models we calculate show that both the generation of converted waves and the apparent velocities of the "oblique" arrivals are sensitive to the dip. In fact dip can be calculated from oblique wave properties. In the next section we model the "oblique" arrivals using optical (high frequency approximation) ray theory. In the last section we analyze examples from the Michigan data and compare these with other logs.

MODELING OBLIQUE EVENTS

The generation of oblique events is related to acoustic discontinuities, either bed boundaries or fractures. In our modeling, our goal is to account for the slope of the events on iso-offset sections. This slope has the dimension of a velocity. We shall refer to it as an apparent velocity and use the notation v_a. Ray tracing provides us with a way to understand what is happening from the standpoint of arrival times. Amplitudes would be harder to determine, and this is not included in our present study. The source-receiver spacing is larger than a wavelength (a minimum of 1 m vs 30 cm), so that we can neglect near field effects. We shall also assume that Snell's law is applicable. Figure 3 shows the various geometric configurations of rays that are transmitted across and reflected at interfaces.

HORIZONTAL INTERFACES

Transmission across a bed boundary

In this case, the tool is astride the discontinuity (Figure 3A). Only the waves transmitted through it are recorded. In the case of body waves, the direct arrivals are compressional waves emitted at the source in the borehole fluid and critically refracted in the formation. These travel as headwaves in the formation and are critically refracted back in the fluid to excite the receiver.

We now assume that a wave travelling in the formation with a velocity v_0 is converted at the interface into another type of wave travelling with a velocity v_1. This wave will arrive some time between the direct wave of velocity v_0 and the one of velocity v_1 such as P to S conversion. This conversion will give rise to an oblique event whose apparent velocity is :

$$v_a = (v_1^{-1} - v_0^{-1})^{-1} \qquad (1)$$

Note that the apparent velocity is independent of the source receiver separation.

This phenomenon is somewhat similar to what happens at a sharp boundary between two different lithologies; the tool averages the velocities over its length and the record shows a ramp in the arrival times. The apparent velocity obeys the same formula as above. In this case no conversion occurs and the same type of wave is propagated through at a different velocity.

One should note that this phenomenon may yield very high apparent velocities. Let us consider, for instance, the case of a boundary between a carbonate with v_p = 22 kft/s and v_s = 12 kft/s and an evaporite such that v_p = 14.5 kft/s and v_s = 9 kft/s. In this situation, the event will have a slope, $(dz/dt = (1/v_0 - 1/v_1)^{-1})$ of 42.5 kft/s for the P- to P-wave transmission event and of 36 kft/s for the S- to S-wave event. Moreover, a conversion from P- to S-wave will have an apparent velocity of 15.2 kft/s, whereas the reverse, from S- to P- wave will reach a tremendous 69.6 kft/s.

Reflection

When the tool is completely above or below the interface (Figure 3B), some of the rays are reflected back to the receiver. These waves are delayed relative to those following the direct path. With the geometry shown in Figure 3 the extraneous path travelled by the reflected waves is twice the separation between receiver and reflector, thus the apparent velocity is

$$v_a = v_0/2 \tag{2}$$

Since we shall discuss dipping interfaces later, let us consider the situation where a conversion occurs at the boundary. In that case, half of the path is travelled at v_0 and the other half at v_1, the velocity of the converted wave. Thus, the apparent velocity would be:

$$v_a = (v_1^{-1} + v_0^{-1})^{-1} \tag{3}$$

General pattern

To illustrate the oblique events, we consider a simple geometry with one source and one receiver only. Let us consider a single horizontal interface as shown in Figure 4. As the tool moves toward and across the interface, different sets of transmitted and reflected events are generated.

When the recording tool is run up the hole, with the transmitters at the top of the tool, the source meets the discontinuity first. Before the source reaches the discontinuity the receiver sees only the direct arrivals and the reflections. When the transmitter is above the interface, the raypaths cross the interface. When the tool has been moved an amount equal to the spacing, the receiver is then above the discontinuity and reflections can occur again. Hence, on iso-offset sections, a single interface will give rise to two symmetric reflection patterns, a tool length apart, amidst which transmission patterns may be seen.

Oblique events start at discontinuities or at a tool length from discontinuities. To start an interpretation, one must look for paired events and locate the discontinuity. To do so, it is advantageous to compare sections with various spacings and correlate other logs with a section. One can discriminate between reflection and transmission and address the right model. We now understand that a single heterogeneity may give rise to a large number of oblique events, even when only a restricted number of wave types are involved. The theoretical pattern for two waves is shown in Figure 4.

DIPPING INTERFACES

Dipping interfaces considered hereafter are plane interfaces intersecting the borehole with an angle α with respect to the vertical. We shall denote apparent theoretical velocities computed for horizontal interfaces with v_{90} and those for dipping interfaces with v_α.

Transmission

The situation is that of Figure 3C. Transmissions with conversion on a dipping discontinuity are modelled using simple ray theory. The details of the model are given in Appendix A.

A useful parameter is $V = v_0 / v_1$. In the appendix, calculations were carried out only for the case $V < 1$. In this case, transmission occurs on the part of the plane nearest to the transmitter. This is the geometrical configuration displayed in Figure A-1. These results can be transposed to the case where $V > 1$. In this situation, the geometry is that of the previous case where receiver and transmitter have been interchanged and the raypaths reversed with the conversion paramenter $1/V > 1$. Since there is very little dependence on the source location, the travel time curve and apparent velocity remain the same.

For the geometry shown in Figure A-1, we consider two cases:

1) $V < \cos\alpha$. Over the span of the tool, the arrival time of the transmitted wave varies between t_0, arrival time of the quickest body wave considered, and t_2 ,

$$\frac{t_2}{t_0} = V\cos\alpha + \sqrt{1 - V^2}\sin\alpha \qquad (4)$$

The apparent velocity varies slowly with the position of the tool and one can approximate its value, v_α, with the following formula :

$$\frac{v_{90}}{v_\alpha} = \frac{V\cos\alpha + \sqrt{1 - V^2}\sin\alpha - V}{1 - V} \qquad (5)$$

2) $V \geq \cos\alpha$. In this case, the situation is much the same as for a horizontal interface.

$$v_\alpha = v_{90}$$

Those results are presented in Figure 5 as well as in Figure A-2. One should remember that, unless we deal with waves such that $\cos\alpha < v_0/v_1 < 1/\cos\alpha$, a dipping interface will increase the apparent velocity of any transmission event. In the case of conversion from P to S wave or vice versa, this phenomenon should only appear for values of α less than 55° , meaning a dip angle greater than 35°, if formation Poisson's ratio is $\nu = 0.25$ or $v_p / v_s = \sqrt{3}$.

Reflection without conversion

Again, the tool is completely above or below the discontinuity (Figure 3D). We modelled this case in Appendix B using the simple geometry of Figure A-3. An exact analytical solution can be worked out. As opposed to the horizontal interface case,

the apparent velocity is now a function of the distance to the reflector and the dip angle. A useful parameter is obtained by scaling the vertical distance to the source receiver separations. Let us then define $z = Z/S$. Z varies between 0 and 1. The angle α is taken with respect to the vertical.

$$\frac{v_a}{v_{90}} = \frac{\sqrt{1 + 4z(z-1)\sin^2\alpha}}{(2z-1)\sin^2\alpha} \qquad (6)$$

The travel time curves are non-linear, but their curvatures are small for small dips. The apparent velocity varies very quickly with dip angle. This phenomenon may yield very high apparent velocities, up to five times the formation velocity for a dip angle of 70°. Figure 6 presents a plot of v_a/v_{90} versus α. Figure A-4 displays identical plots for various values of z. These curves are located between the curves $1/\sin\alpha$ and $1/\sin^2\alpha$, corresponding to the limiting cases of $z = \infty$ and $z = 1$.

We shall take advantage of the sensitivity of the apparent velocity for the dip angle to determine dips. From the previous remarks, we expect to have a good angle resolution for medium to large dip angles.

Reflections with conversion

A body wave travelling in the formation at the velocity v_0 impinges on a plane boundary, dipping from the vertical with an angle α, and is reflected back toward the receiver with the velocity v_1 (Figure 3E). Convenient parameters are $V = v_0/v_1$ and z, the vertical distance from the source to the discontinuity normalized with respect to the source-receiver spacing, S. This case is modelled in Appendix C.

We computed the arrival time and apparent velocities in the situation where the tool is completely above the discontinuity. Using the symmetry of the problem, we can transpose the results to the situation where the tool is below the discontinuity at a distance $z < 0$ from it. In such a case, the results are similar to those in the previous case obtained for the parameters $1/V$ and $1 - z$. That is : $v_a(\alpha, V, z) = v_a(\alpha, 1/V, 1-z)$. The general behavior of the apparent velocity is very similar to that obtained for reflection without conversion. Let us look at two cases.

1) $V < \cos\alpha$. In this situation, when the tool is completely above (or below) the discontinuity, the reflected wave arrives along the interface at the receiver at time t_2, as defined in equation (4), earlier than the direct arrival. The reflection point is some distance from the borehole. As the tool is pulled up, the reflection point moves back into the formation. The closer V is to $\cos\alpha$, the smaller the movement, and the smaller the variation in arrival time. Hence, the apparent velocity will increase with V.

2) $V \geq \cos\alpha$. The reflected wave arrives at the receiver at the same time as the direct arrival when the tool is just completely above the interface and the reflection point is on the borehole wall. When the tool is pulled upward, this point recedes further into the formation; the greater the V, the further it recedes. The apparent velocity will then decrease.

Thus, for a given angle, the apparent velocity will present a maximum for $V = \cos\alpha$ as we can see in Figure 7. It follows that for a given geometry, two different values of V will yield a single value for v_a/v_{90}. In Figure 8 we show v_a/v_{90} plotted versus α for given values of V. These curves are shifted to higher apparent velocity as V increases. This trend is reversed for $V \geq 1$. In this case we

obtain slowly varying curves, very similar to those obtained when no conversion occurs. The curves are much more sensitive to V when $V < 1$ because of the possibility of having a grazing emergence in this situation. Moreover, these curves will intersect one another due to the occurrence of the maximum described previously.

Unlike the horizontal interface case, for a dipping interface the apparent velocities of the reflections for a tool above or below the interface will not be the same. For large z, the apparent velocities tend to decrease for a given angle of dip.

Scattering point analogy

The problem of transmitted and reflected events can be viewed as a diffraction problem. In the case of an interface normal to the borehole, the loci of diffracting points are rings around the borehole. A scattering point becomes a secondary source when excited by an incident wave from the transmitter. Conversion phenomena can be taken into account by setting an outgoing velocity different from the incoming one.

When the scattering point sits right next to the borehole wall, the model yields a single hyperbolic arrival time curve (Appendix D) and one finds in the limit exactly the same results as those found in the previous sections dealing with horizontal interfaces, that is, in the way we analyzed it in the previous parts, two reflection events "linked" by a transmission event. Figure 9 displays the travel time curves obtained with a scattering point embedded in the formation at one-tenth of the source-receiver spacing for three velocity ratios. If no conversion occurs, the transmitted event corresponds to the direct arrival. If a conversion occurs, we have two reflection branches with an apparent velocity close to $(v_0^{-1} + v_1^{-1})^{-1}$ and a transmission branch with an apparent velocity close to $(v_0^{-1} - v_1^{-1})^{-1}$. For a scattering point deeper in the formation (Figure 10), the travel time curve is shifted toward later times and becomes smoothed out yielding higher apparent velocities.

The point that we want to emphasize here is the continuity between the two reflections and the transmitted event. A similar analogy can be made for the dipping interface.

Since any type of wave can, theoretically, be converted into any other type, we expect complex features from real data. Surface, pseudo-Rayleigh, and Stoneley waves are, by definition, restricted to the borehole wall. However, at an interface they could scatter into both body (P and S) and guided waves. Such diffraction patterns have been observed where fractures intersect the borehole (Mathieu and Toksöz, 1984 report).

ANALYSIS OF REAL DATA ACQUIRED BY EVA

In this section we analyze EVA data from the Burch well in Michigan. The tool was run at a slow speed that enabled us to study oblique events over a 1000 foot thick section of the well. We chose two examples for detailed analysis.

(1) The Brown Niagaran formation (see Figure 1) shows a number of oblique events that can be produced by a single discontinuity in a rather homogeneous formation.

(2) The second one consists of the sharp interface between the A-1 carbonate and the A-2 evaporite (see Figure 1).

Conventional logs corresponding to the section studied are presented in Figure 11.

Before going into detailed analysis we will briefly discuss the data processing method used to enhance the oblique events.

DATA PROCESSING AND EVALUATION

Since oblique events are the result of reflection, conversion, and transmission travel paths, they are generally weaker in amplitude than "regular" arrivals. In order to achieve an accurate detection and a good determination of the slope of these events we need to separate them from the main wavefield. In formations where velocities vary slowly with depth, the main wavefield is roughly horizontal (infinite apparent velocity) whereas reflection and transmission events show finite apparent velocity. The F-K filtering technique allows us to extract oblique events that we are interested in. We can go further and extract two given types of wave using the method of separation described by Seeman and Horowicz (1983).

Velocity filtering

Velocity filtering is a widely used technique in seismic processing that can be readily applied to iso-offset sections. However the following conditions have to be satisfied.

1) Constant logging speed is required in order to achieve constant spatial sampling.

2) Cut-off velocities must be chosen in order to preserve the highest finite apparent velocities. The optimization may be different for different formations and at different arrival times on the section.

3) Spatial aliasing must be avoided to guarantee accurate results from filtering algorithms. This leads to the constraint that the spatial sampling must be less than $\Delta Z(Nyquist) = v_a / 2Fmax$ for all types of waves. This condition requires generally a very dense spatial sampling.

Let us consider, for example, reflections from a horizontal interface involving P and Stoneley waves in a hard formation. The upper frequency of the P wave is close to 25 kHz whereas the Stoneley frequency is less than 6 kHz. The P and Stoneley wave velocities are 20 kft/s and 5.6 kft/s which yield reflected events with apparent velocities 10 kft/s and 2.8 kft/s. In both cases the theoretical minimum sampling rate is close to 2.5 inches. However, a practical upper bound of 4 inches still provides good numerical results.

Figure 12 shows results obtained when appling a symmetrical fan filter to the EVA section of Figure 2. Despite the high cut-off velocity required to preserve the transmission events, the filtering has strongly enhanced oblique events. A second example is presented in Figure 13. Again, velocity filtering allows us to pick obiique arrivals more precisely.

Separation of waves

Unambiguous interpretation of interfering events sometimes requires further processing to separate events with different velocities. A good approach is the method used in VSP to separate the up- and downgoing waves. The method is based on the assumption that each recorded signal is the superposition of two coherent waves with different apparent velocities and a random component. The solution is obtained by a least square minimization of the residual wavefield in the frequency domain. This technique requires the picking of travel times of the two events we want to separate.

Figure 14 shows results of this separation applied on the previously "dip-filtered" data of Figure 13. As expected, the two main signals we were able to pick are well separated. Furthermore, the residual error shows two weak events we were unable to detect even on filtered data.

Separation techniques are very useful to study a given type of wave and to detect possible weak events. The method can be extended to any number of waves (Panziera and Arens, 1985), and therefore would be more appropriate in our case.

EXAMPLES

Example 1

The full waveform section of the Brown Niagaran formation is displayed in Figure 2. The source-receiver spacing is 12.75 meters. We shall concentrate on the events at depth 4900 ft, shown in enhanced form in Figure 12.

By comparing sections with various spacings we note that the events originating at about 4900 ft stay at the same location, whereas, those at the 4860 ft depth move with the different values of the spacing. Thus the complex pattern is generated by a single discontinuity located at 4900 ft. The events at depths deeper than 4900 ft and shallower than 4860 ft are reflections and the intermediate ones are transmissions. These transmissions are the first indication of a dipping interface.

These events start at the arrival time of either the P arrival or the S arrival at the 4900 ft depth, and end respectively at the S arrival or P arrival at 4860 ft a spacing length apart. Their measured apparent velocities are about 24.6 kft/s. With v_P = 20.8 kft/s and v_S = 11.3 kft/s, the theoretical apparent velocity is 24.7 kft/s. Several reflections can be seen originating either from the P or S arrival. We designate them by R_P or R_S. We have two R_P and two R_S reflections. They are defined by their apparent velocity in the table. In addition to the slight curvature affecting R_{P1} and R_{S2}, and the fact that some of the velocities are much higher than those we would get from reflections on a horizontal plane, we infer the presence of a dipping boundary.

To determine the dip angle, we have to compute the v_{90}'s , apparent velocities yielded by a reflection on a horizontal reflector for each possible situation.

Reflection of a P wave without conversion : 10.4 kft/s

Reflection of an S wave without conversion : 5.65 kft/s
Reflection P to S wave and vice versa : 7.3 kft/s

Now, for each of the reflections, we determine the ratio of the apparent velocity to the corresponding v_{90} and then derive the angle α.

TABLE 1

		No Conversion	Conversion
	v_a	$v_a/10.4$	$v_a/7.3$ with V=1.8
R_{P1}:	13.0 kft/s	1.25→59°	1.78→38°
R_{P2}:	9.7 kft/s	0.93→90°	1.33→52°
		$v_a/5.65$	$v_a/7.3$ with V=0.5
R_{S1}:	11.1 kft/s	1.96→40°	1.52→53°
R_{S2}:	7.0 kft/s	1.24→59°	0.97→90°

Discussion

From the values in Table 1, we come up with a set of three possible angles. One set of data gives $\alpha = 90^\circ$ (i.e., a horizontal interface). This case, which does not exclude having a dipping reflector, only means that the reflection occurred very close to the borehole wall.

The remaining angles are close to either 40° or 55° within reasonably small intervals. The question is : which one of those two will account for ALL the measured apparent velocities ?

We notice first that angles close to 55° appear four times in the table whereas the other value is approached only twice. Furthermore, R_{P2} and R_{S2} can be explained in two ways, considering reflections either on a horizontal interface or on a dipping reflector with $\alpha = 55^\circ$. Both events are also stronger than their faster neighbors. Finally, the transmission event matches very well the theoretical apparent velocity for the horizontal interface situation. From our modelling, we know that this can only happen when $V=v_0/v_1$ is greater than or equal to cosα. In our case, V=0.54 yields an angular limit of 57°. In conclusion, we believe that a correct estimation for α is 55°, meaning a dip angle of 35°.

The final results of the interpretation are indicated in the table below. The question mark underlines the ambiguity of having a conversion on a horizontal interface.

TABLE 2

event		wave type before		wave type after reflection	angle
R_{P1}	:	P	→	P	yes
R_{P2}	:	P	→	P	no
	:	S	→	P	yes
R_{S1}	:	P	→	S	yes
R_{S2}	:	S	→	S	yes
	:	P	→	S	no?

Example 2

The iso-offset section for Example 2 is displayed in Figure 15. Spacing is 12.75 meters. We shall concentrate on all events related to the sharp boundary at depth 4750 ft.

The velocity of the compressional wave for the A-1 carbonate is about 21.7 kft/s, whereas, for the A-2 evaporite, it is 15.0 kft/s. The shear velocities are, respectively, 12.6 and 8.7 kft/s. The caliper log indicates a change in the borehole radius from 8 in to 14 in when passing from the carbonate to the evaporite (see Figure 11). This may account for the very strong events recorded.

Five reflections can be seen on the filtered section in Figure 13: from the P arrival an oblique event with the apparent velocity of 12 kft/s and a second one at about 5 kft/s; from the S arrival, one at 6.6 kft/s, a second at 4.2 kft/s and a third one at about 3 kft/s. A sixth event has been detected in the P arrival using the technique of separation (Figure 14, event 3), with the apparent velocity 8.3 kft/s These six events have been sketched in Figure 16.

With the given formation velocities, the theoretical apparent velocities are : 10.85 kft/s for the P- to P-wave reflection and 6.3 kft/s for the S- to S-wave reflection. These values yield ratios, v_α / v_{90}, between 1.1 and 1.05 for the quickest events originating from the P and S direct arrivals. The corresponding events may then be interpreted as reflections on a dipping interface whose α is about 75°, meaning a dip angle close to 15°.

The event detected by applying separation corresponds to the S to P conversion, with the theoretical apparent velocity 7.97 kft/s. Again, the ratio v_α / v_{90} is about 1.04. It is consistent with the estimated dip.

The remaining velocities are too small to be explained by reflections involving body waves only. We need to take into account slower surface waves. As a consequence of this, these reflections occur in the vicinity of the borehole wall. We have reflections of the Stoneley wave converted into a P-wave, yielding the

apparent velocity of 5 kft/s, and also converted into a S-wave, yielding the apparent velocity of 4.2 kft/s. The Stoneley wave is also reflected without conversion, explaining the event at 3 kft/s.

These velocities are a little high compared to the theoretical ones computed from a velocity of the Stoneley wave of 5.6 kft/s: respectively, 4.5, 3.9 and 2.8 kft/s. Nevertheless, they are not high enough to permit considering any body waves. An alternative would be to consider the first mode of the pseudo-Rayleigh wave. It happens in the laboratory. In either case, we should note the strong effect of the borehole radius variation on a surface wave. A non negligible amount of its energy is being reflected back, either directly or converted into body waves.

The properties of the evaporite do not fully appear as long as the receiver has not left the carbonate. This produces sloping events whose apparent velocities can be worked out in a similar fashion as for transmission with conversion. This part forms a "transition zone". We also find transmission with conversion events related to the sharp interface: A P- to S-wave conversion yielding a measured apparent velocity of 67 kft/s, compared to a theoretical 78.7 kft/s. The S- to P-wave conversion is also visible at about 12 kft/s, versus a theoretical 14.5 kft/s. The record presents also S- to Stoneley wave conversions with a measured apparent velocity of 12.5 kft/s to be compared to a theoretical 15.7 kft/s for a velocity of the Stoneley wave of 5.9 kft/s. Here, the agreement is relatively poor. As a matter of fact, multiple interferences in the transition zone made the picking of the events difficult. Moreover, the theoretical expression for transmission events is particularly sensitive to small formation velocity variations.

CONCLUSIONS

After step by step modelling of different cases most likely to occur within a layered medium, we tried to show the consistency between transmission events and reflection events in the case of a horizontal interface as well as in the case of a dipping interface. We also presented numerous events that can be associated with a single discontinuity. From our modelling of dipping interfaces, one should remember that they increase the apparent velocity of the events relative to the value obtained with a horizontal interface. One can take advantage of the relative increase to derive dip angles. It illustrates also that one can think of retrieving some lateral information from full waveform acoustic logging data, and should add to the on-going efforts of fracture characterization. Since oblique events are most likely to occur at interfaces with high impedance contrast, fractures could be studied by this method.

The examples presented show that the real data could be very complex. We observed the general patterns that one can predict from theory. We were able to match the slopes of oblique events and determine the dip of each interface. These dips are consistent with dip-meter data as shown in Figure 17.

Data processing, velocity filtering and separation of events enhance the oblique events and improve the accuracy of the results.

ACKNOWLEDGEMENTS

The work has been conducted independently both at the Well-Seismic Department of SNEA(P) and at the Earth Resources Laboratory, and reached identical conclusions. B. Paternoster and M. Larrère are ELF Aquitaine fellows at M.I.T.

REFERENCES

Biot, M.A., 1952, Propagation of elastic waves in a cylindrical bore containing a fluid: Journal of Applied Physics, 23, 977-1005.

Cheng, CH., and Toksöz, M.N., 1981, Elastic wave propagation in a fluid-filled borehole and synthetic acoustic logs: Geophysics, 46, 1042-1053.

Koerperich, E.A., 1978, Investigation of acoustic boundary waves and interference patterns as techniques for detecting fractures: J. Petro. Tech., 1199-1207.

Panziera, J.P. and Arens, G., 1985, Three component vertical seismic profiles -- polarized wave separations: submitted to the 55th Ann. Meeting of the SEG.

Schoenberg, M., Marzetta, T., Aron, J. and Porter, R., 1981, Space-time dependence of acoustic waves in a borehole: J. Acoust. Soc. Am., 70, 1496-1507.

Seeman, B. and Horowicz, L., 1983, Vertical seismic profiling: separation of upgoing and downgoing acoustic waves in a stratified medium: Geophysics, 48, 555-568.

Serra, O., 1984, Fundamentals of Well-Logging Interpretation, vol. 1, The Acquisition of Logging Data, chap. 15, 247-250, Elsevier.

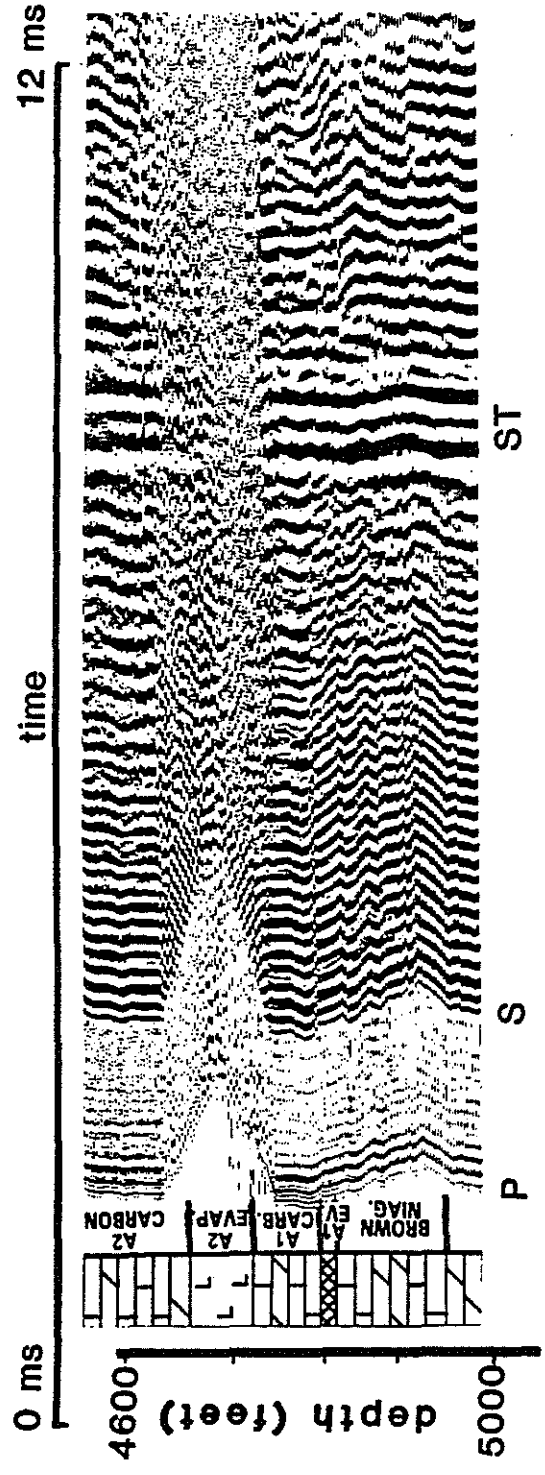

Figure 1. Iso-offset section from EVA tool. The spacing is 12.75 meters.

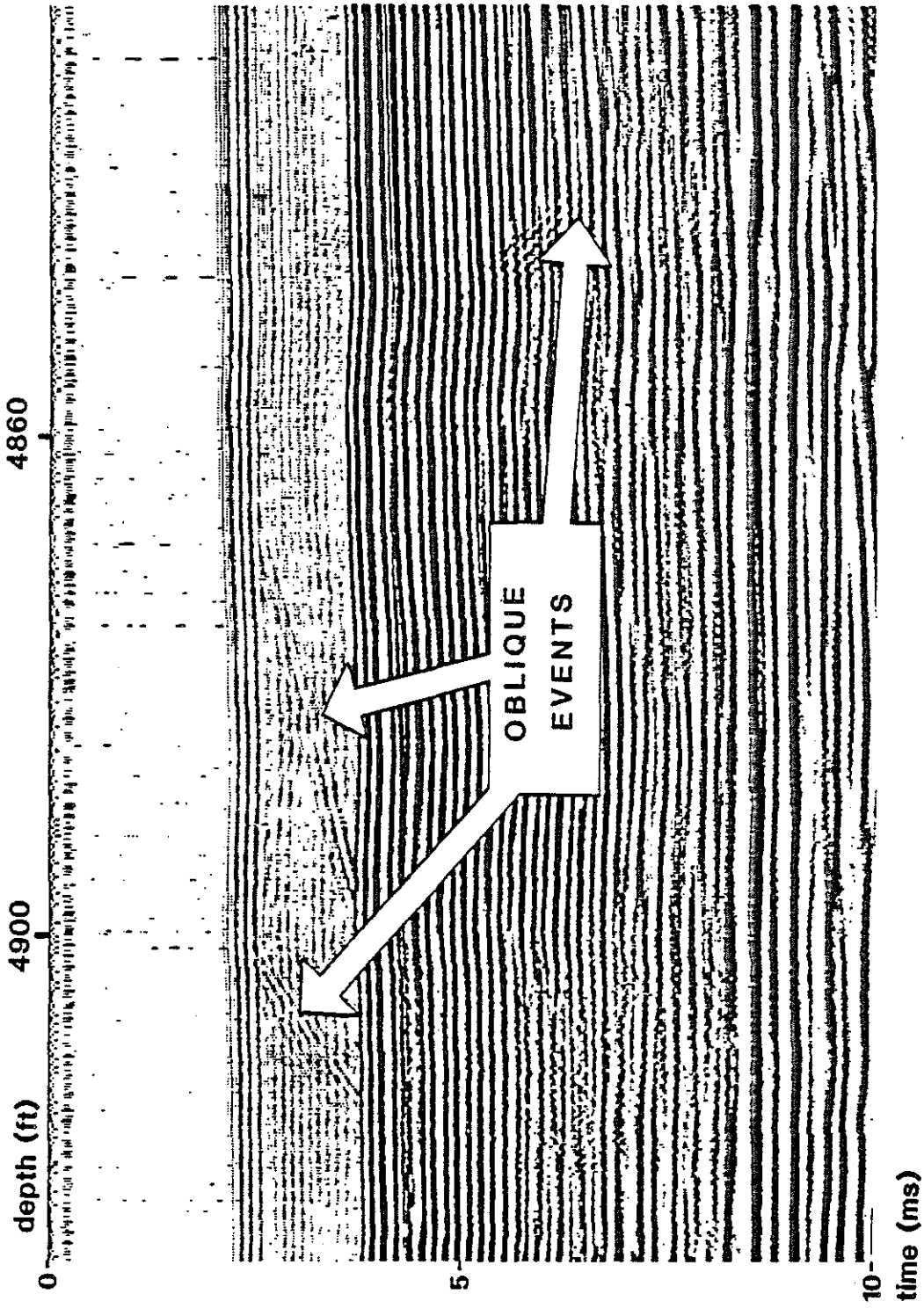

Figure 2. Oblique events on iso-offset section.The spacing is 12.75 meters.

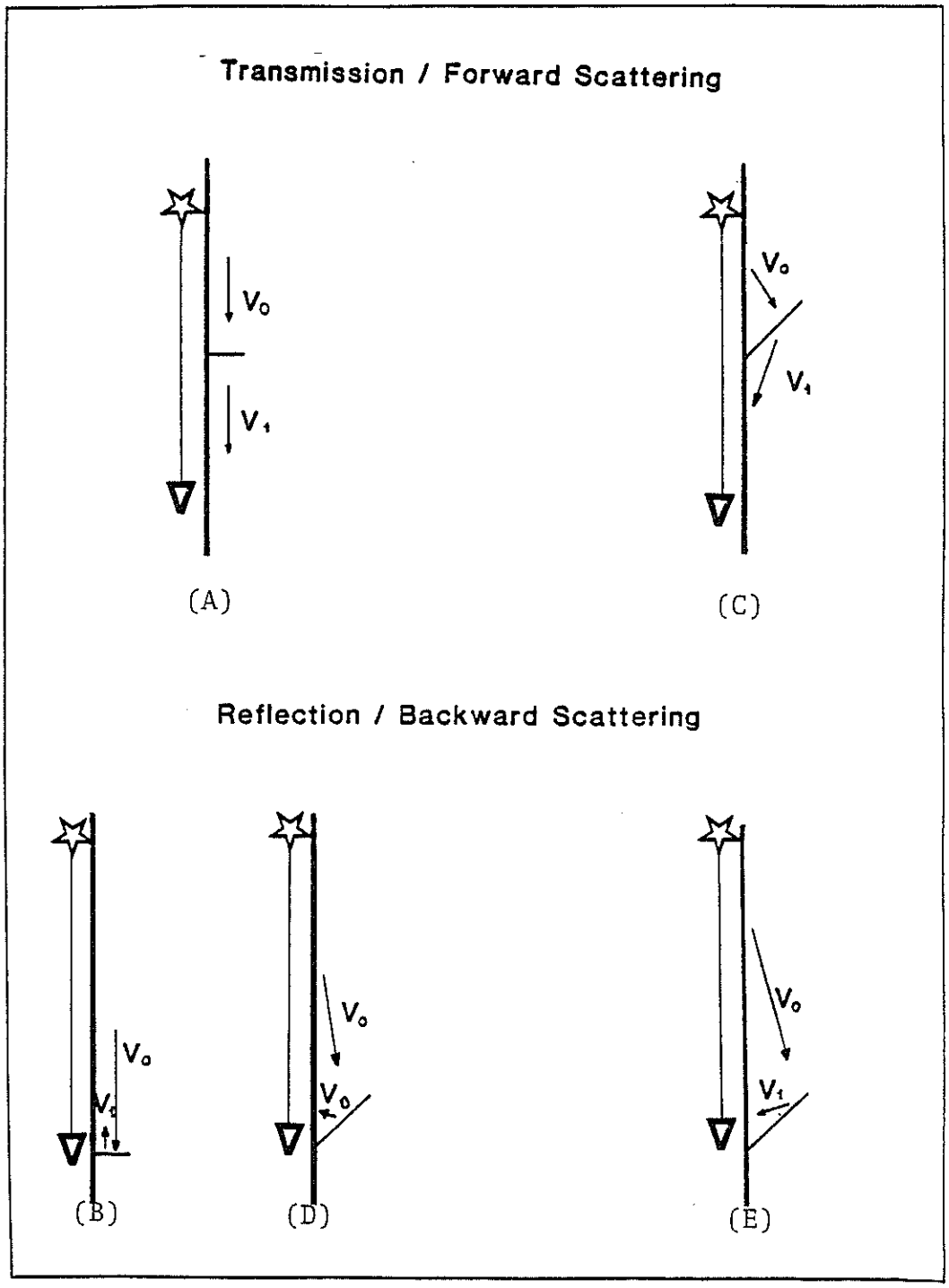

Figure 3. Geometric configurations modelled in this paper. The source is on top of the tool.

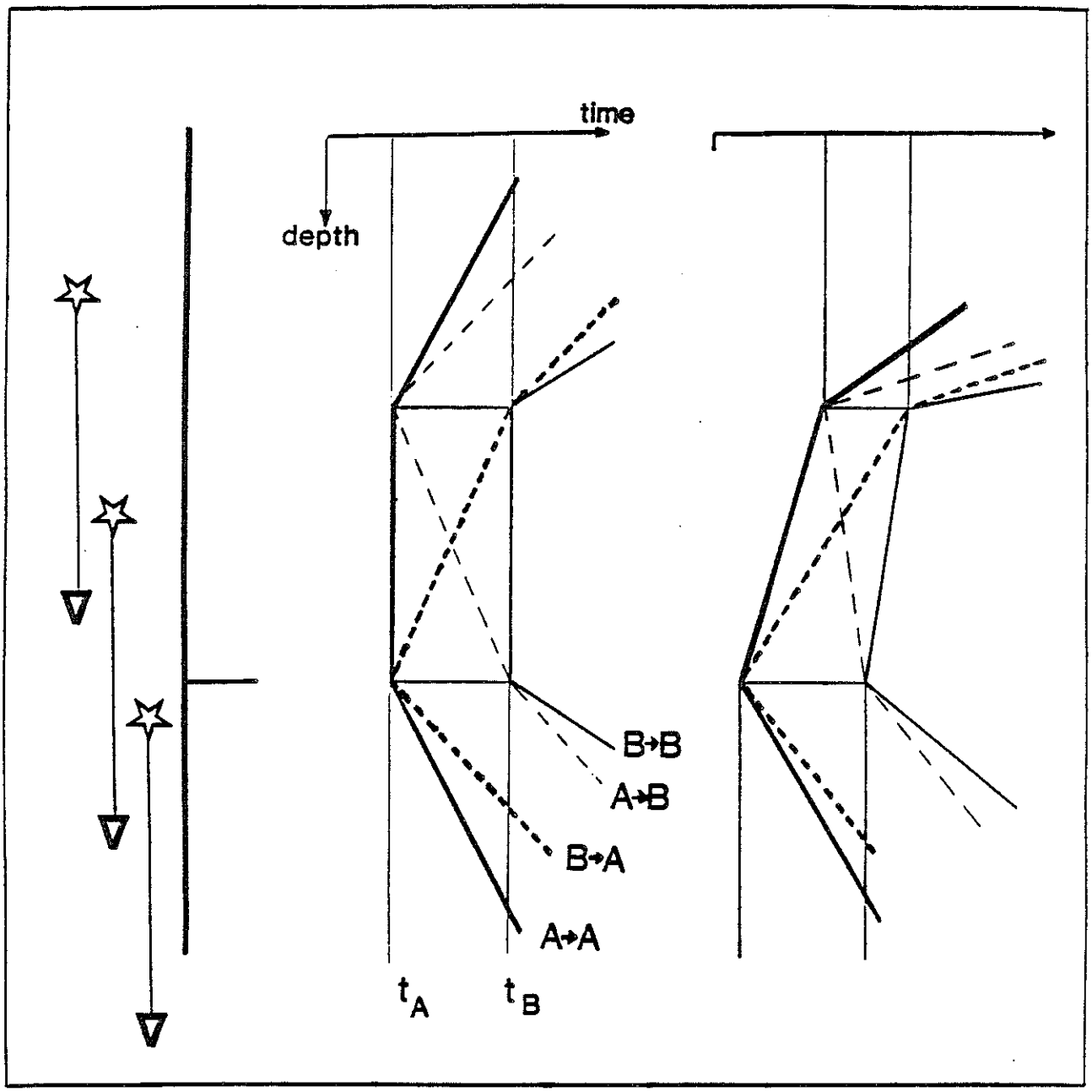

Figure 4. Schematic iso-offset sections displaying the events that can be produced by a single discontinuity involving all possible combinations between only two types of waves noted A and B. The lefthand side of the figure corresponds to an heterogeneity embedded in an homogeneous formation while the righthand side corresponds to the case of a sharp interface.

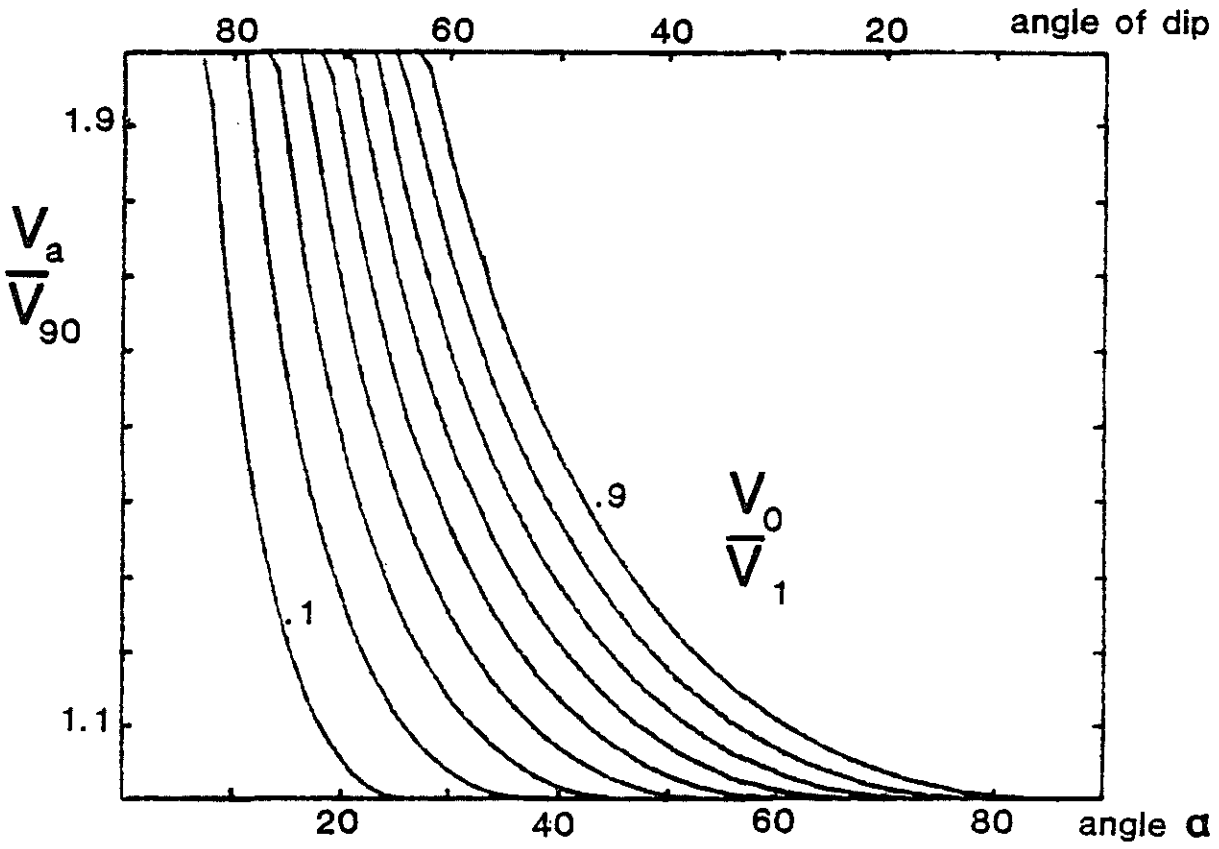

Figure 5. Normalized apparent velocity, v_α / v_{90}, resulting from the transmission with conversion through a dipping plane intersecting the borehole with an angle α to the vertical. Plots have been drawn for velocity ratios (velocity of the incoming wave over the velocity of the outgoing wave, v_0 / v_1) ranging from 0.1 to 0.9.

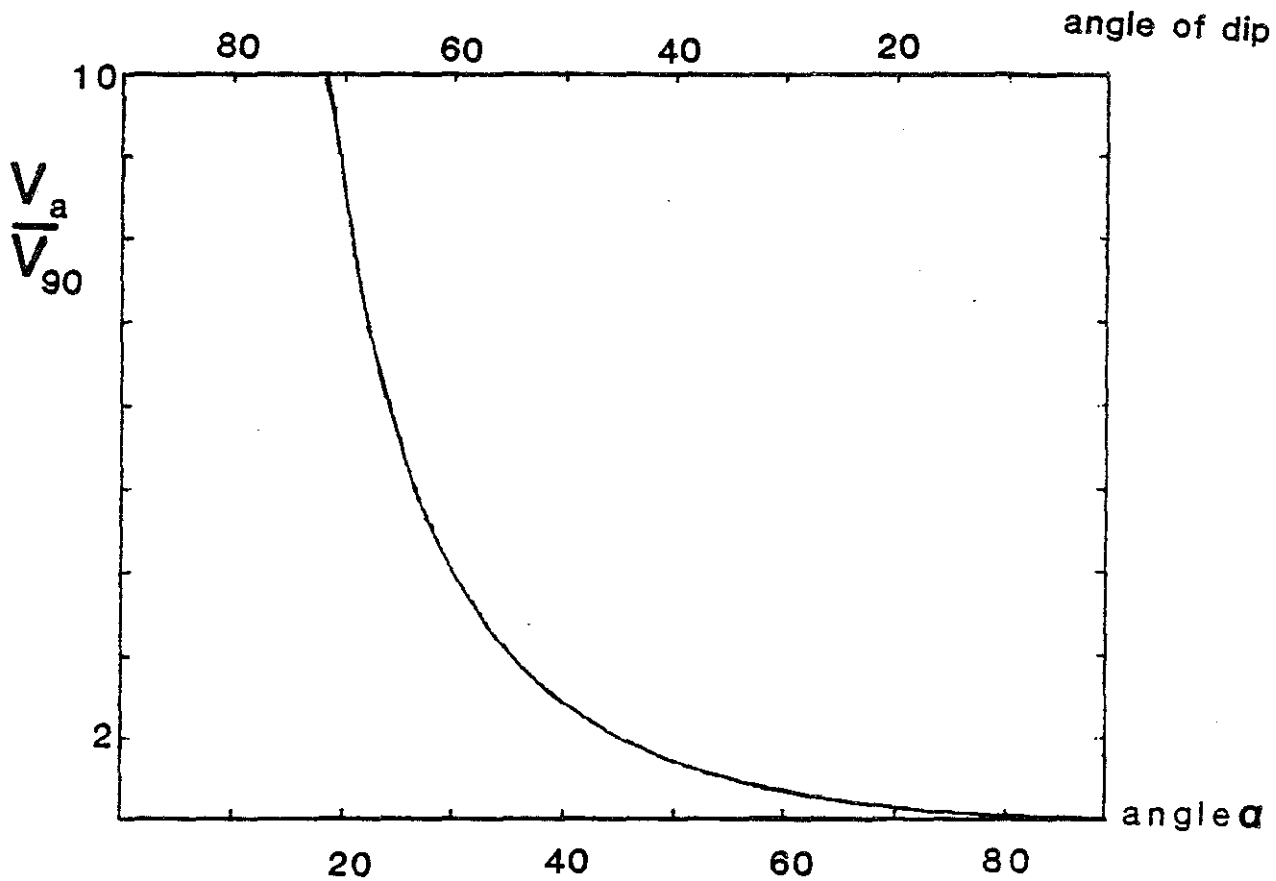

Figure 6. Plot of the apparent velocity v_a, normalized to half the formation velocity versus the angle of dip at z=1 for a reflection without conversion on a dipping plane interface.

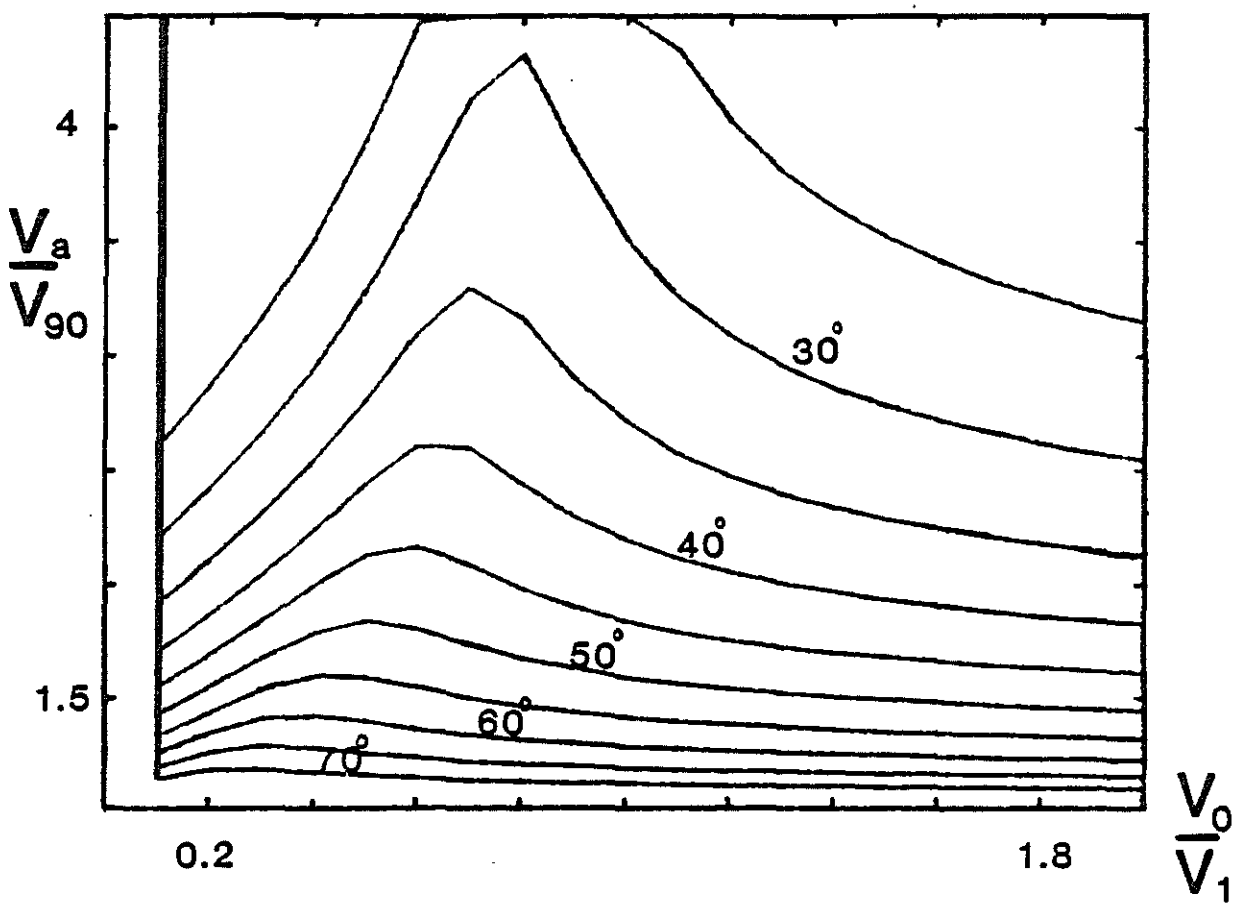

Figure 7. Normalized apparent velocities obtained for a reflection with conversion on a dipping plane interface. Velocities are plotted versus the velocity ratio determining the conversion, v_0/v_1, for given angles α ranging from 25° up to 70°. Each curve has a maximum at $\cos\alpha$.

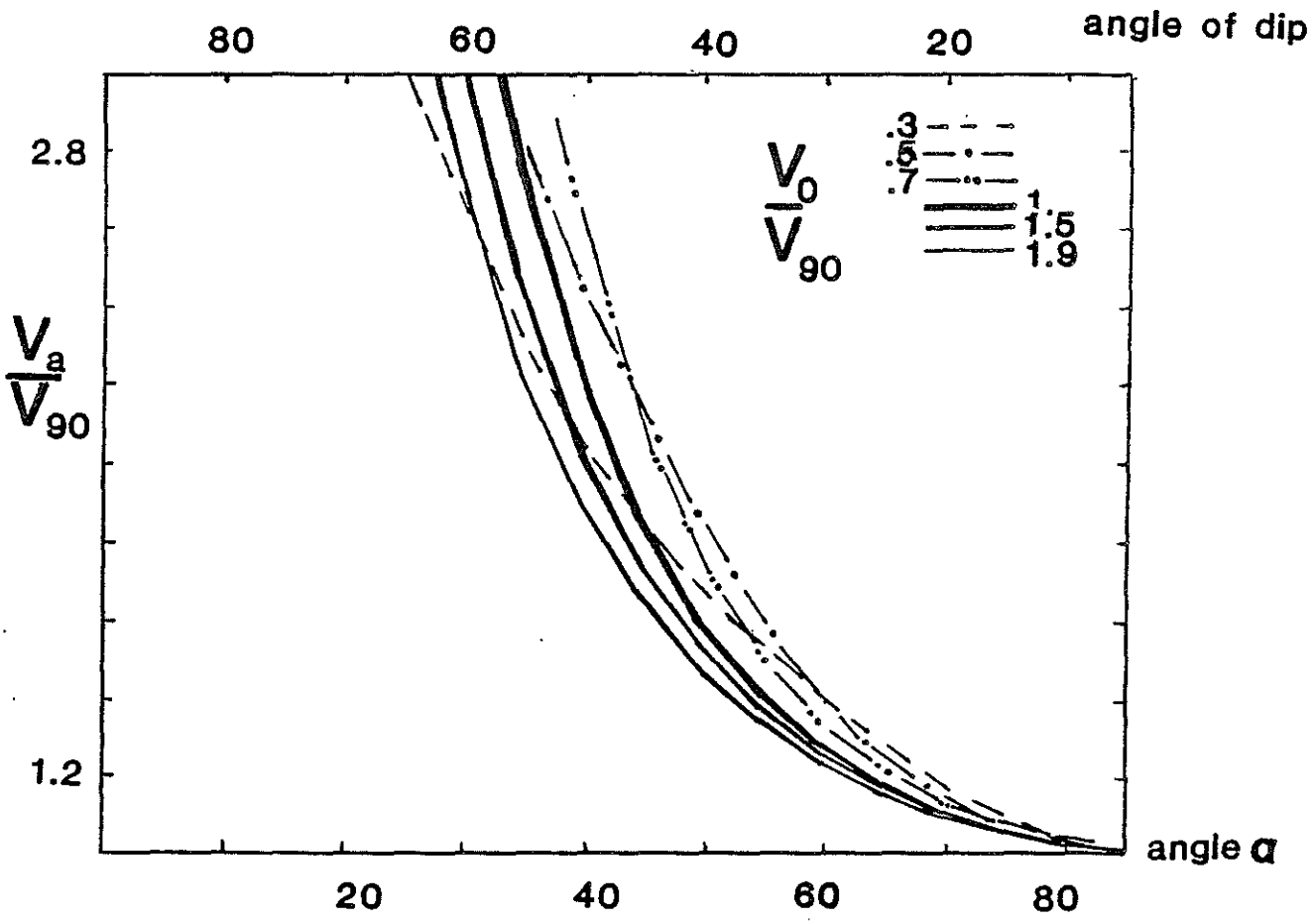

Figure 8. Plot of the apparent velocity obtained for a reflection with conversion on a dipping plane interface. The velocity is normalized with respect to the apparent velocity in the horizontal plane case and plotted versus the angle of dip for given velocity ratios determining the conversion.

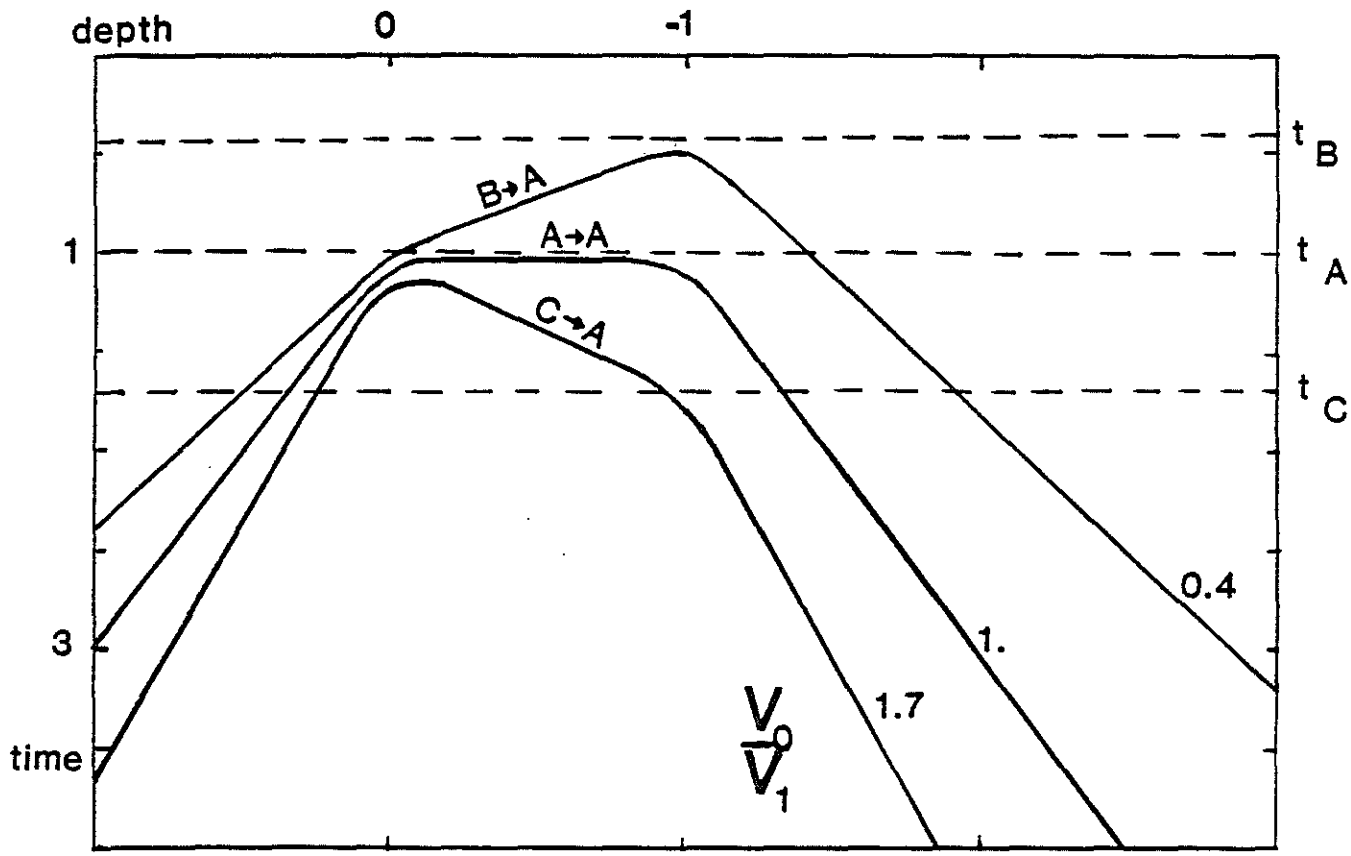

Figure 9. Travel time curves obtained from a scattering point in the formation. Depth units are in spacing length. The point is at depth 0 and .1 deep in the formation. Time units are in t_A, arrival time of the wave of type "A". Two types of conversion have been considered and noted $B \rightarrow A$ and $C \rightarrow A$, corresponding to velocity ratios, V, of 0.4 and 1.7.

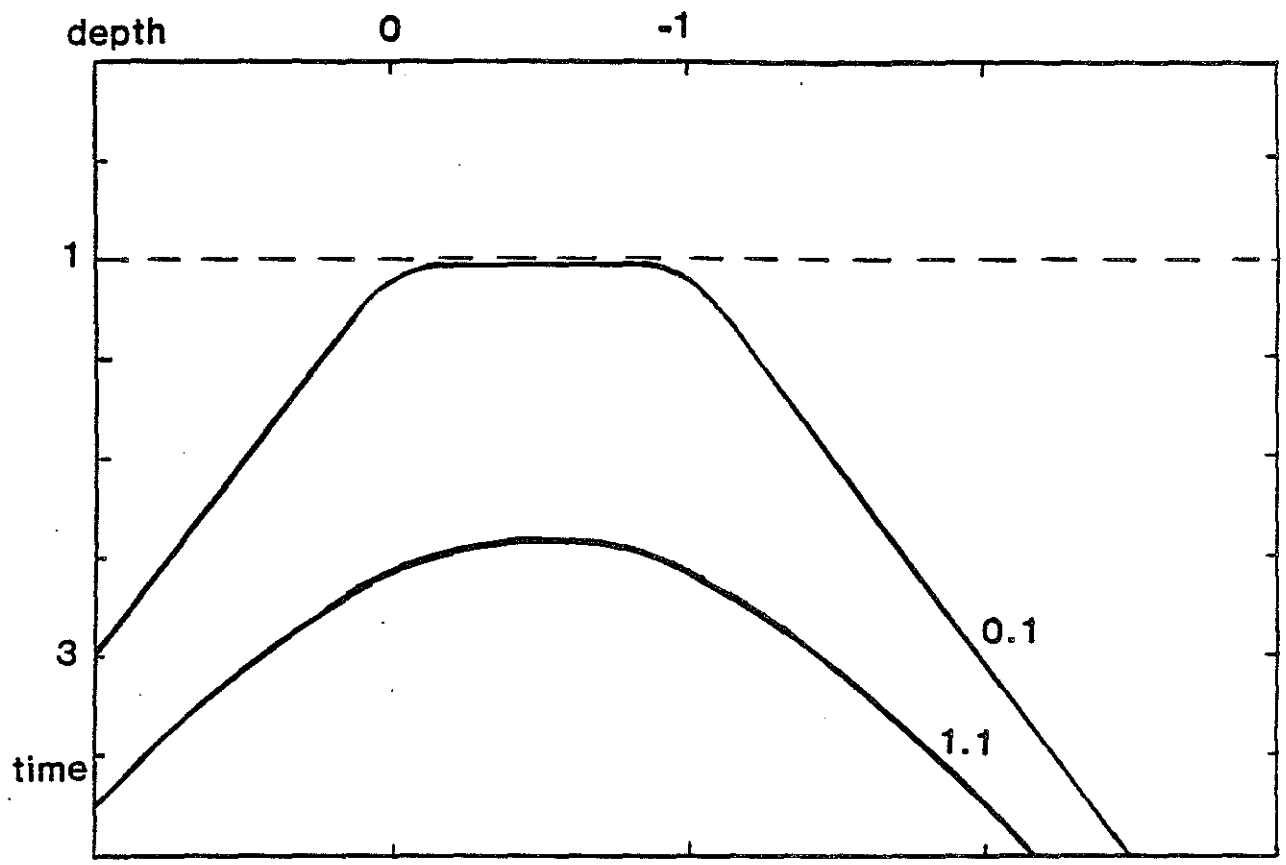

Figure 10. Travel time curves obtained from a scattering point. Conversions have not been considered. The point is 0.1 or 1.1 deep in the formation. The apparent velocities are smoothed out and increased.

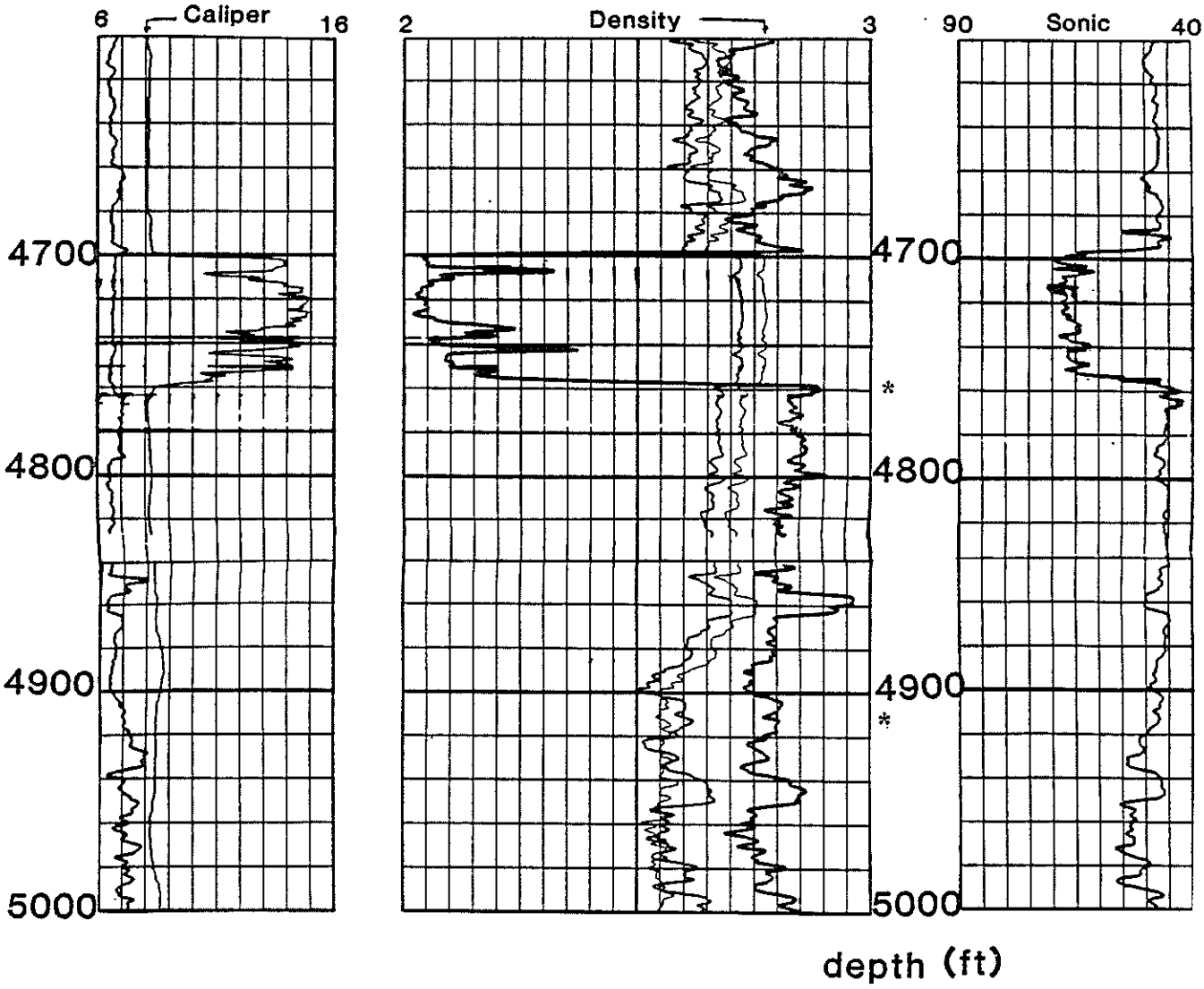

Figure 11. Section of the logs run in the studied well. Location of the two examples choosen for detailed analysis are indicated by a star label.

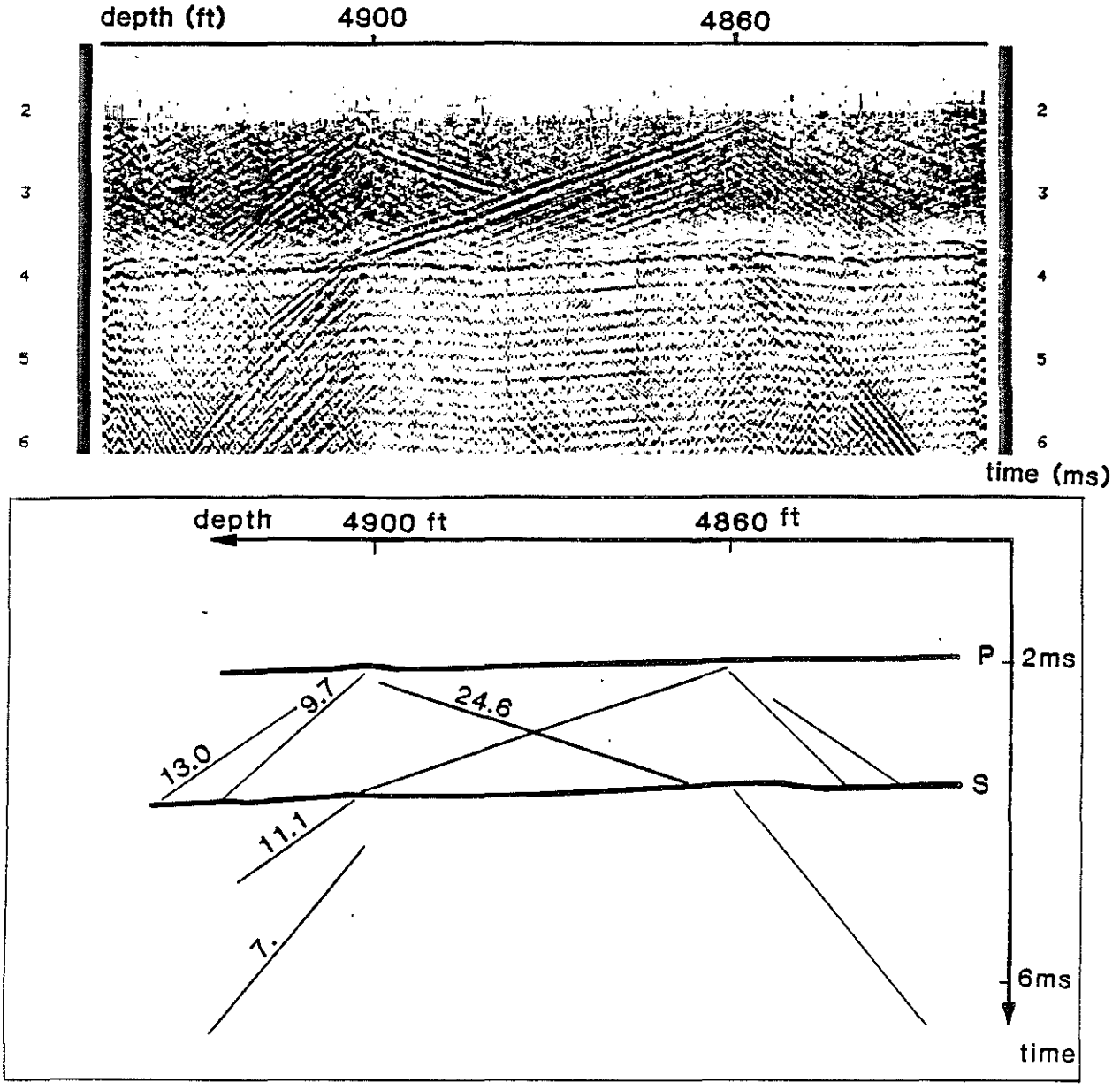

Figure 12. Iso-offset section of Figure 2 after fan-filtering and schematic sketch of the events with apparent velocities in kft/s.

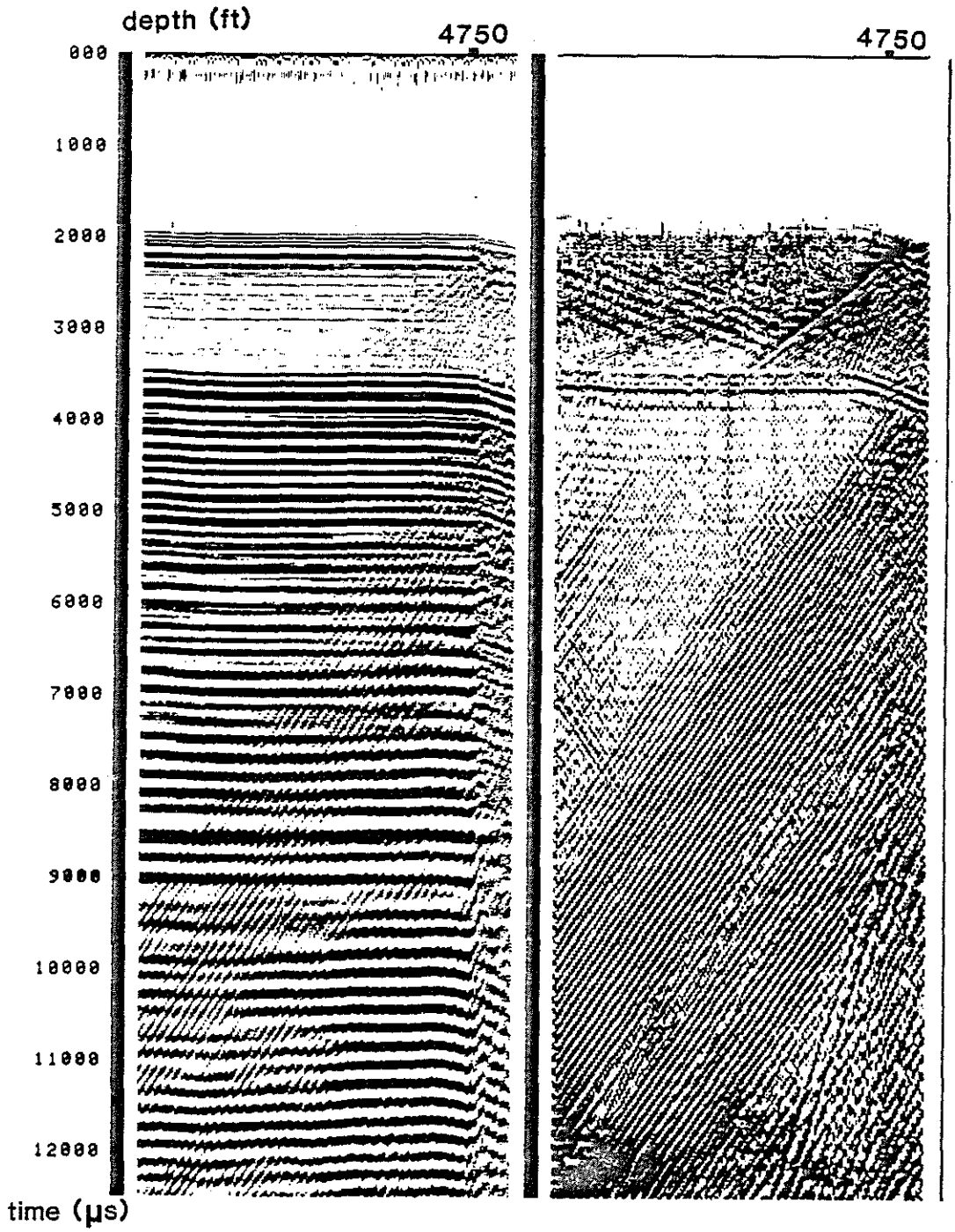

Figure 13. Iso-offset sections before and after fan-filtering.

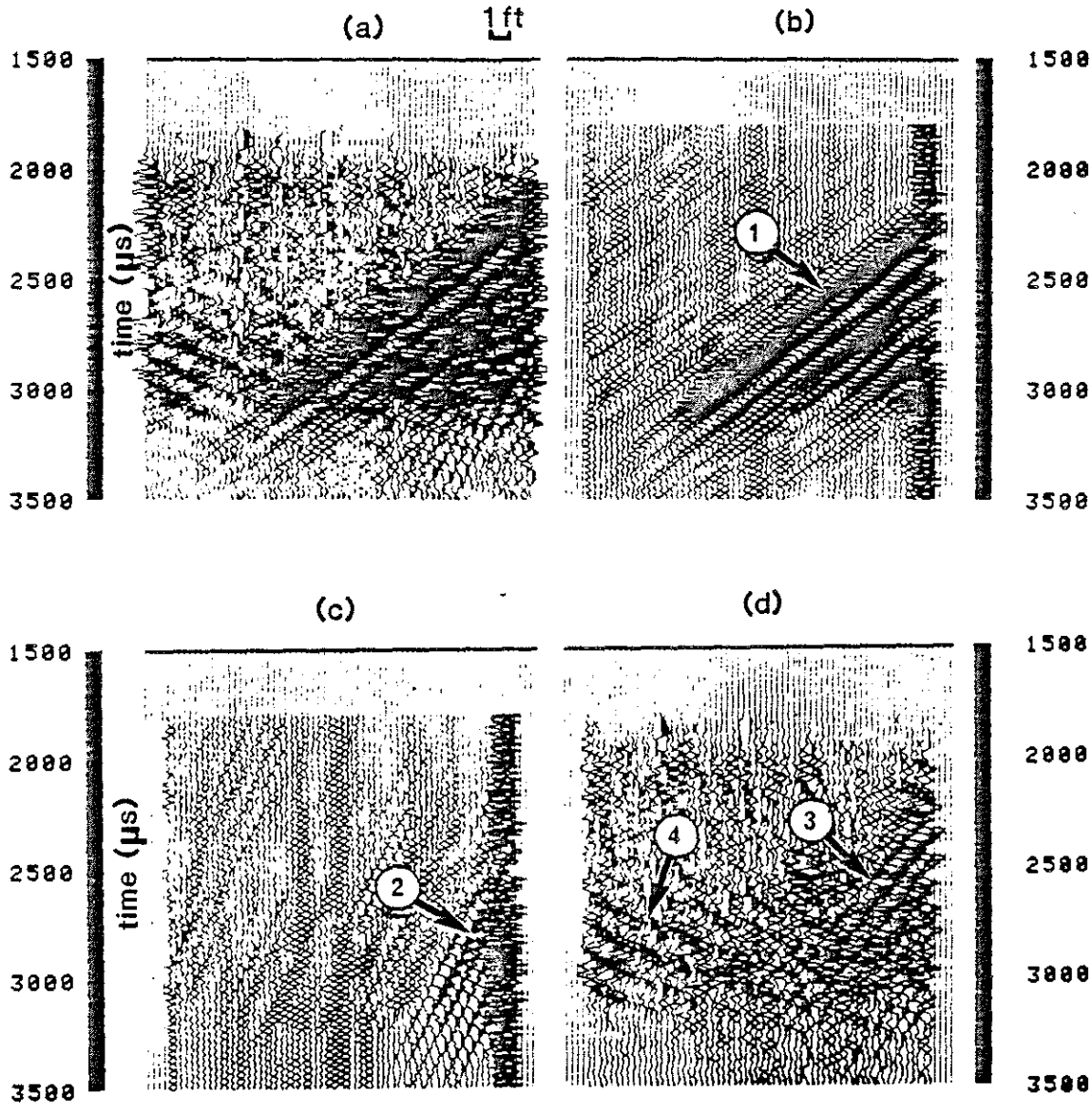

Figure 14. Example of separation. Events 1, in (b), and 2, in (c), are extracted from (a). The residual wavetrain (d) shows two weak arrivals. Notice that event 3 was invisible in (a). (Event 4 is related to a different discontinuity).

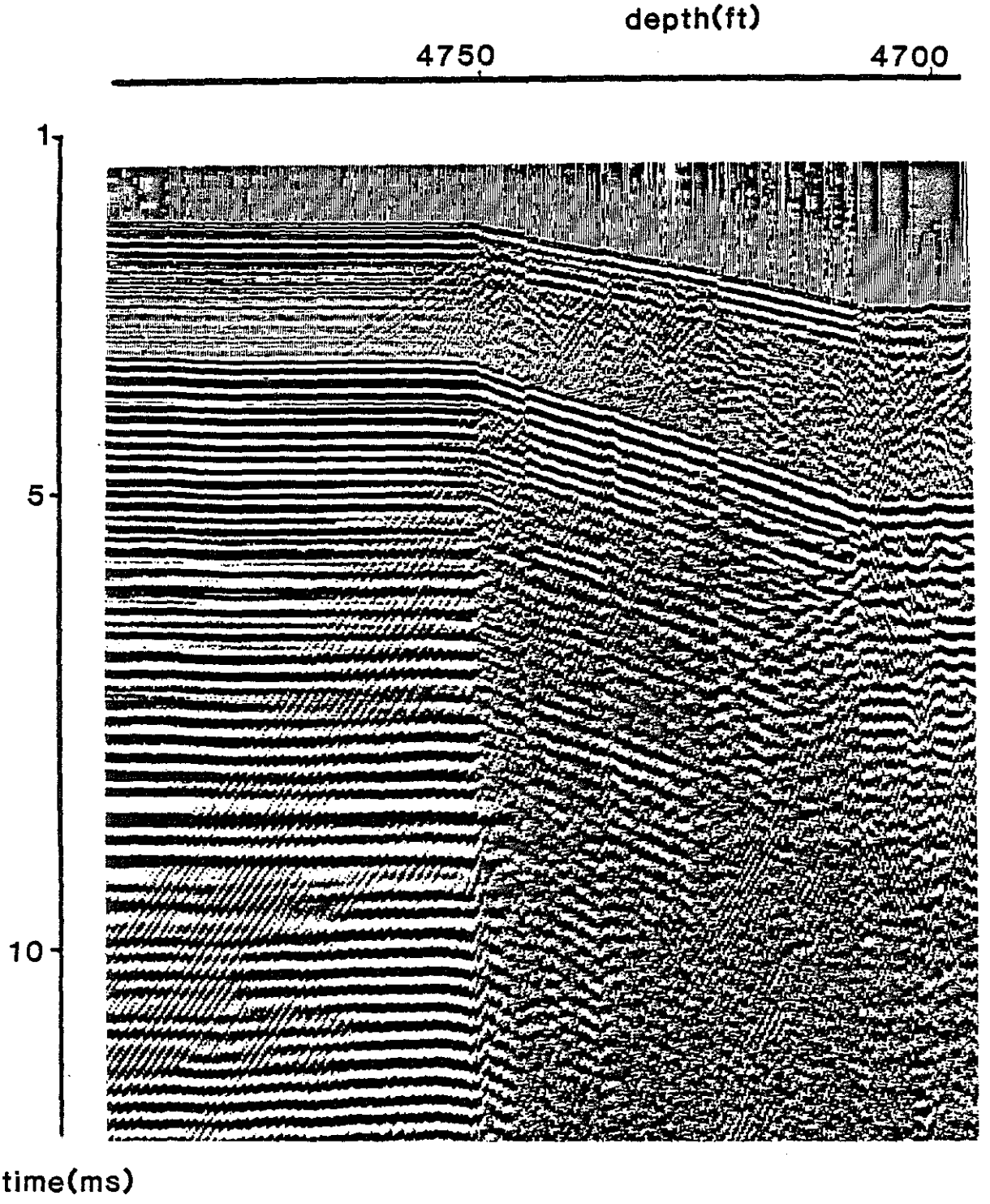

Figure 15. (Example 2) Iso-offset section from EVA for a 12.75 meter source receiver separation.

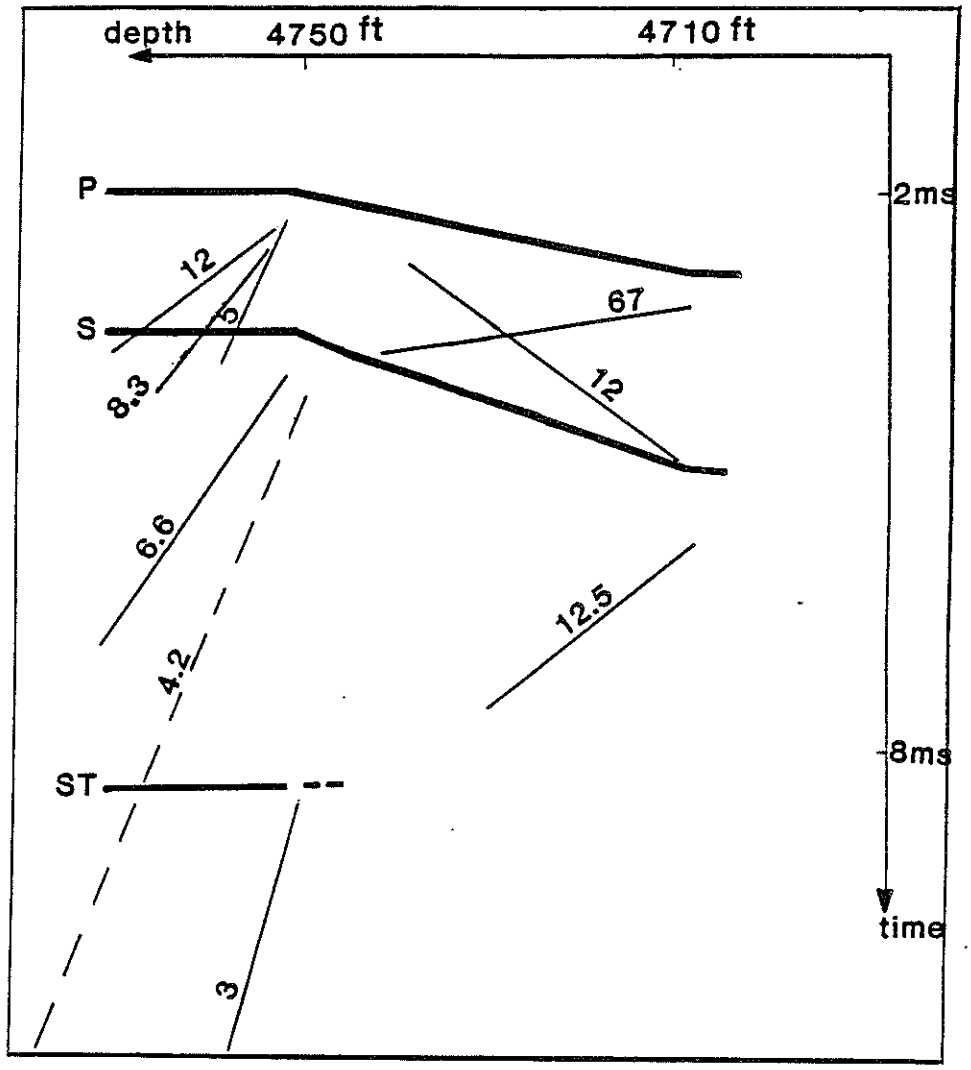

Figure 16. Sketch of the events presented in the text corresponding to the iso-offset section in figure 15.

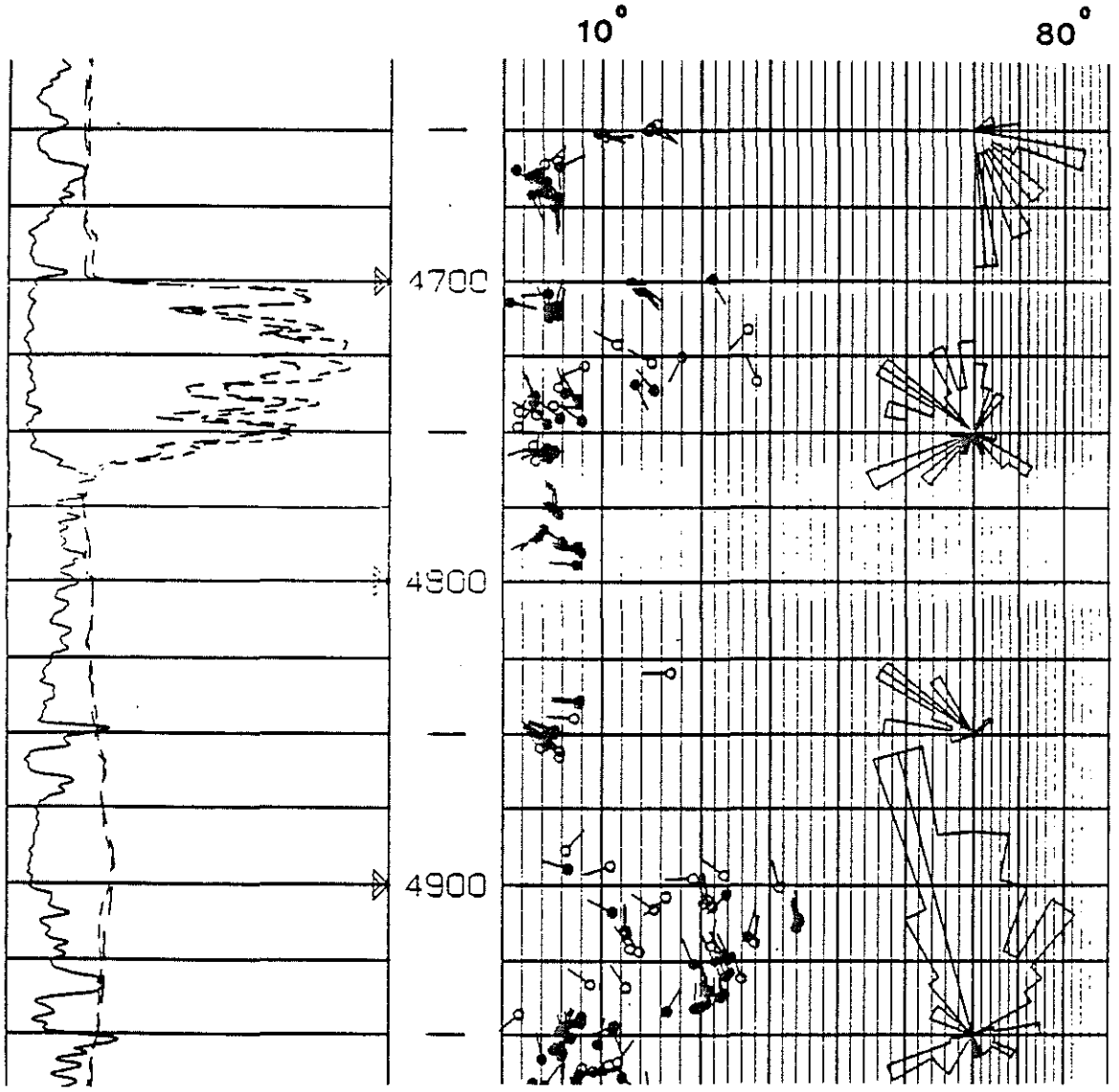

Figure 17. Dipmeter data for the section of the well covering examples 1 at depth 4900 ft and 2 at depth 4750 ft.

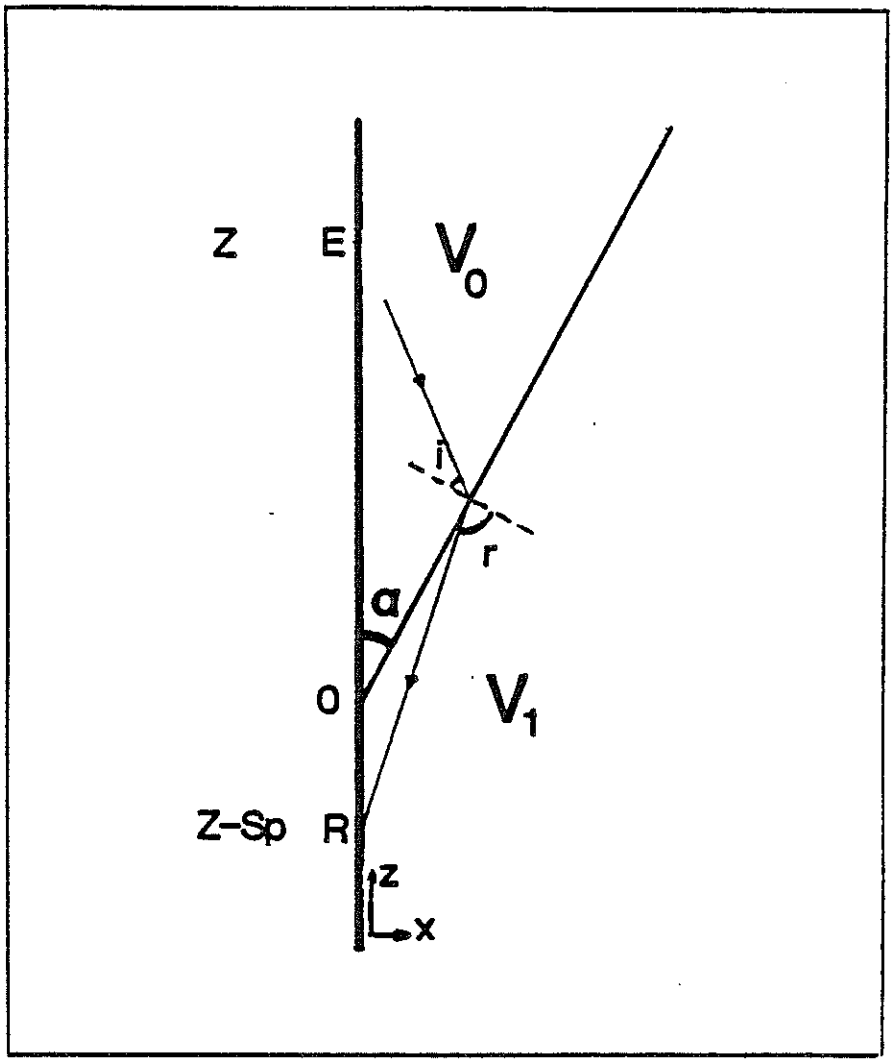

Figure A-1. Geometrical configuration in the case of Appendix A for a transmission with conversion through a dipping plane interface. The source is on top of the tool. In this situation, v_0 is larger than v_1.

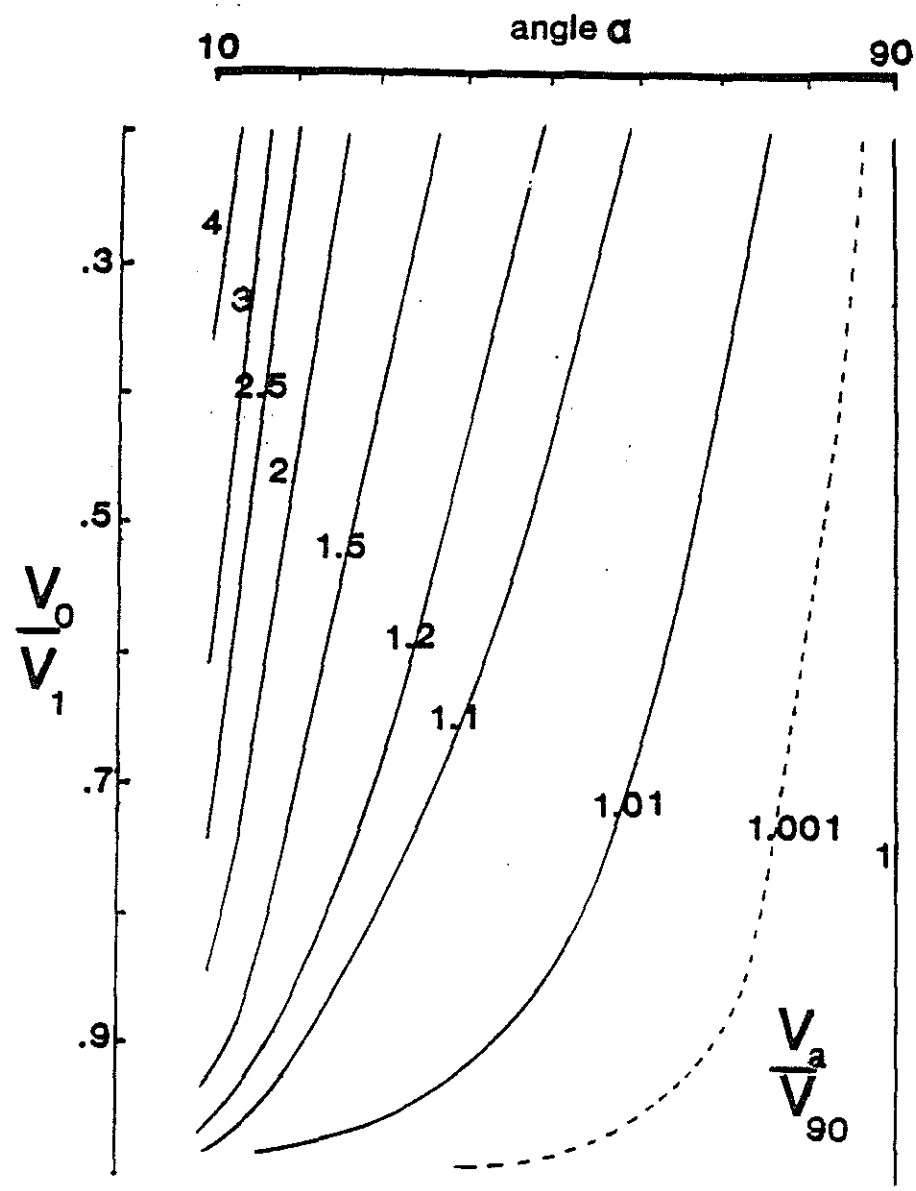

Figure A-2. Transmission with conversion through a dipping plane interface case. Isovalue curves for the average of v_α / v_{90} in the (α, V) plane, that is in the plane angle versus velocity ratio v_0 / v_1. The average is taken for z varying from 0.0 to 0.8.

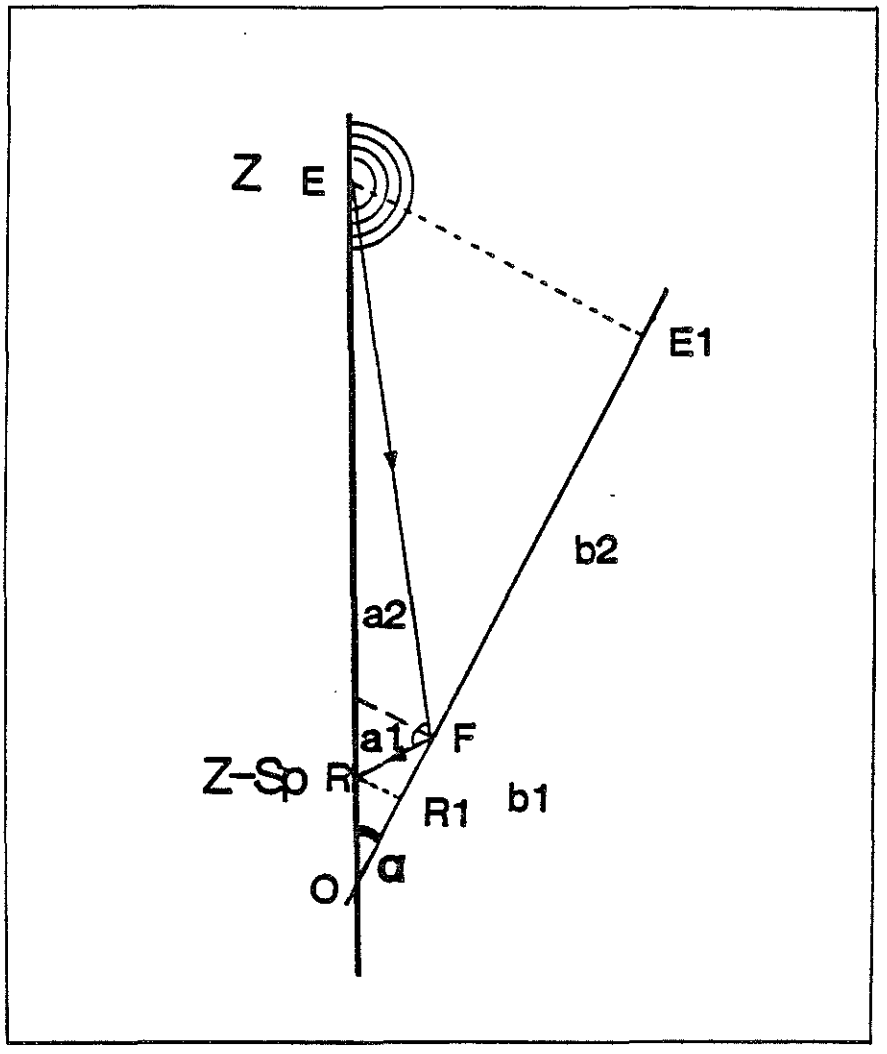

Figure A-3. Geometrical configuration and notations used in Appendix B for the case of reflection on a dipping interface without conversion.

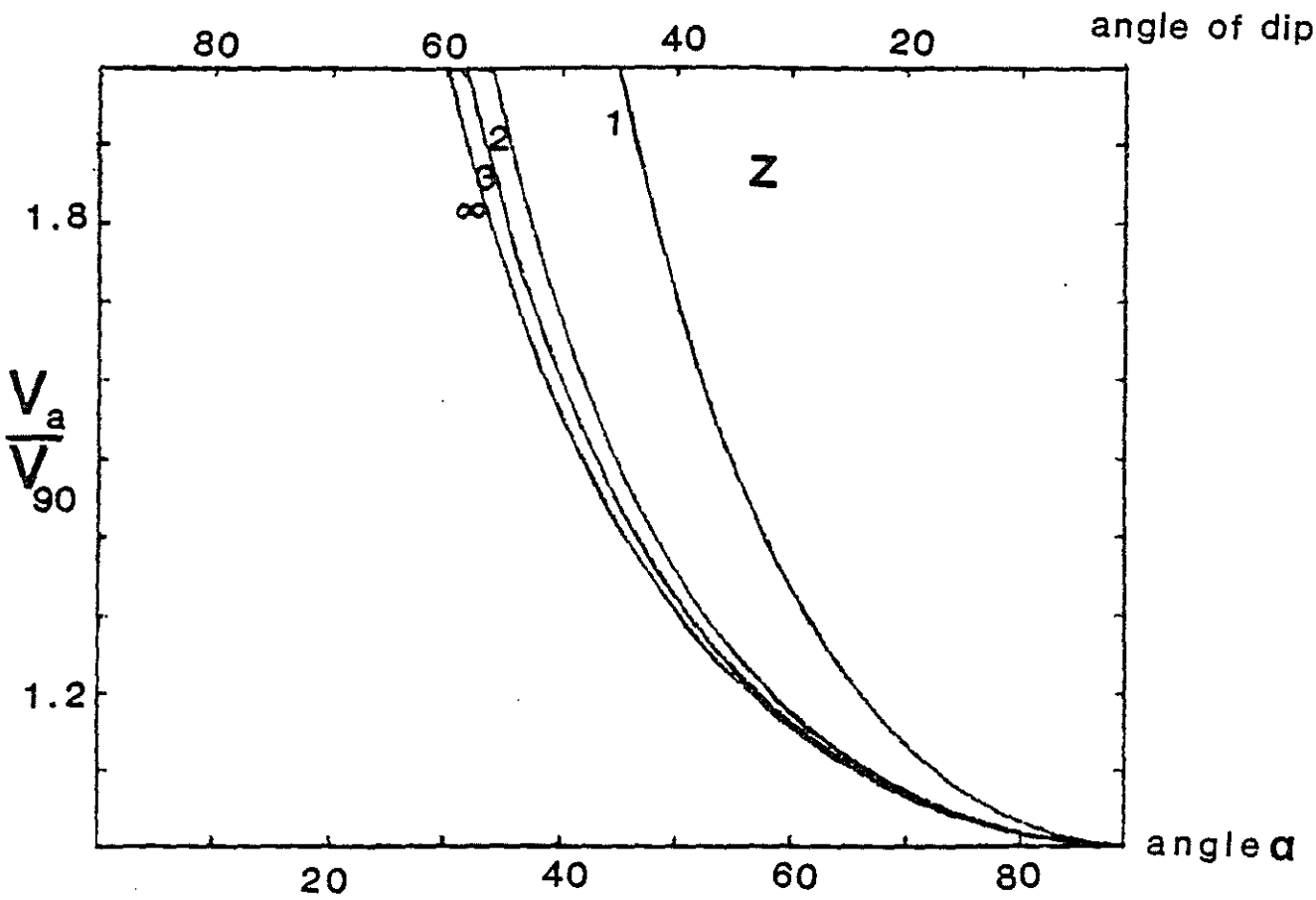

Figure A-4. Plot of the apparent velocity normalized to half the formation velocity versus the angle of dip for a reflection on a dipping interface without conversion. three positions of the tool have been considered, z = 1, 2, 3 and in the limit, ∞.

OBLIQUE EVENTS IN FULL WAVEFORM ISO-OFFSET SECTIONS : APPENDICES

In the following appendices, we consider the simple case of a plane surface intersecting the borehole axis with an angle α. Note that α is the angle between the interface plane and borehole axis. The dip of the interface is $\vartheta = 90 - \alpha$.

The headwaves are refracted from the fluid into the formation. Regular arrivals observed in full waveform logging correspond to critical refraction, and thus to a downward propagation (in the case where the transmitters are at the top of the tool) along the borehole wall in the formation. Nevertheless, a certain amount of energy propagates away and may impinge on any discontinuity, such as a dipping surface. Using this simple geometry enables us to compute approximate raypaths for body waves travelling away from the borehole and being redirected back to it on the discontinuity.

The general scheme is to compute the arrival time using geometrical relations, and derive the apparent velocity differentiating the travel time curve. Whenever conversion occurs, the exact problem is hard to solve analytically and numerical solutions are necessary.

APPENDIX A : TRANSMISSION THROUGH A DIPPING INTERFACE.

Computation of the arrival time

The tool is astride the discontinuity in the geometrical configuration of Figure A-1. This is also the case where $v_0/v_1 < 1$. Due to the conversion, the apparent velocity of that event cannot be computed in a straightforward manner. We have to define at first the point of the interface where transmission occurs. This point is at the intersection of three straight lines in the plane containing the borehole axis and the normal to the reflector. Those lines are :

- The incoming ray
- The outgoing ray
- The trace of the interface in the plane.

We may express the equations of those lines in a system of planar cartesian coordinates with its vertical axis (z) matching the borehole axis and originating at the intersection with the reflector, and an horizontal axis (x). In this system, our three lines are

$$\begin{aligned} z - Z &= -tan(i + \alpha)\cdot x \ ; \\ z - (Z - Sp) &= tan(\pi - r - \alpha)\cdot x \ ; \\ z &= tan(\pi/2 - \alpha)\cdot x \end{aligned} \qquad \text{(A-1)}$$

Where Z is the location of the source, and Sp, the source to receiver separation. The incident angle, i, and the reflection angle, r, refer to the normal to the reflector whereas α denotes the angular separation between the vertical and the reflector.

The lines having a common point, we then have :

$$(Z/Sp)(tan(i + \alpha) - tan(r + \alpha)) = tan(i + \alpha) + tan(\frac{\pi}{2} - \alpha) \qquad \text{(A-2)}$$

Following some trigonometric manipulations, we end up with :

$$\tan\alpha \, [\, (Z/Sp) tan\, i + (1 - Z/Sp) tan\, r \,] = 1 \qquad \text{(A-3)}$$

Snell's law provides us with a second equation :

$$\frac{1}{v_0} \sin i = \frac{1}{v_1} \sin r \qquad \text{(A-4)}$$

We found it more convenient to use V, the ratio v_0/v_1. In the numerical computations, the angles are worked out by tests using these two equations. Hence i and r are supposedly known in the following calculations. Consequently, the arrival time of the wave can be ruled out :

$$\frac{t}{t_0} = \sin\alpha [\frac{Z/Sp}{\cos i} + \frac{(1 - Z/Sp) V}{\cos r}] \qquad \text{(A-5)}$$

t_0 is the arrival time of the headwave, refracted in the formation under critical incidence and propagated in the formation with the velocity v_0 directly toward the receiver, that is, under the assumptions made hereby, Sp/v_0.

Apparent velocity of the arrival.

Equation (A-5) yields an expression (A-6) for the apparent velocity by differentiating both sides with respect to Z or, more conveniently, with respect to Z/Sp. Let $z = Z/Sp$ vary between 0 and 1.

$$\frac{dt}{dz} = t_0 \sin\alpha \, [\, \frac{1}{\cos i} - \frac{V}{\cos r} - (z-1) V \frac{\sin r}{\cos^2 r} \frac{dr}{dz} + z \frac{\sin i}{\cos^2 i} \frac{di}{dz}] \qquad \text{(A-6)}$$

The derivatives of i and r with respect to z can be solved by solving the linear system obtained by differentiating equations (A-3 and A-4). Thus we have :

$$\cos r \frac{dr}{dz} = \frac{\tan r - \tan i}{\frac{zV}{\cos^3 i} + \frac{(1-z)}{\cos^3 r}} \quad \text{and} \quad \cos i \frac{di}{dz} = V \cos r \frac{dr}{dz} \qquad \text{(A-7)}$$

Substituting these two equations in equation (A-6) leads to the final result :

$$\frac{v_{g0}}{v_a} = \frac{\sin\alpha}{1-V}[\cos i - V\cos r] \qquad \text{(A-8)}$$

Where v_a is the apparent velocity that we have been looking for, and v_{g0} the velocity reached for an horizontal interface, namely $v_{g0} = (v_0^{-1} - v_1^{-1})^{-1}$.

Discussion

In the different algebraic simplifications made to get equation (A-8), we avoided difficulties arising as the receiver approaches the discontinuity, a situation where r reaches $\pi/2$. This yields numerical instabilities as z tends to 0 and, sometimes, invalidity. Two cases are to be considered:

$v \geq \cos\alpha$

The possible range for incident angles i does not allow r to reach $\pi/2$, and, the computation can be done. The converted wave arrives at the same time as the direct arrival : $t = t_0$ at $z = 0$ whereas $t = t_1 = Sp/v_1$ at $z = 1$. The computation shows that v_a/v_{g0} is always near unity. This remains consistent with the fact that for large values of V, the point where transmission occurs stays in the vicinity of the borehole.

$v < \cos\alpha$

Equation (A-5) does not allow r to be equal to $\pi/2$ which happens in this case at $z = 0$. The converted wave arrives earlier than t_0 yielding higher apparent velocities. While the tool moves along the borehole, the transmission point remains somehow at the same place, thus leading to an apparent velocity that varies slowly with depth. This enabled us to compute a meaningful average of v_a computed over a limited range of z with the numerical procedure described above.

The results for this computation, restricting z to the interval [0,0.8], are drawn in Figure (A-2) under the form of an iso-value chart for v_a/v_{g0} in the plane α, V. Note that the values should be slightly excessive since the apparent velocity continuously decreases, and since we have averaged over the first part of that small variation.

A second way to present results is to consider that v_a is constant. In such a case, one may use the arrival time at $z = 0$, t_2 :

$$\frac{t_2}{t_0} = V\cos\alpha + \sin\alpha\sqrt{1 - V^2} \qquad \text{(A-9)}$$

Hence the apparent velocity :

$$\frac{v_{g0}}{v_a} = \frac{V\cos\alpha + \sin\alpha\sqrt{1 - V^2} - V}{1 - V} \qquad \text{(A-10)}$$

These results, presented in Figure 5, are consistent with those of Figure A-2.

APPENDIX B: REFLECTION ON A DIPPING SURFACE WITHOUT CONVERSION

The tool is completely below or above the discontinuity. The geometrical problem can be solved directly. Refer to Figure A-3 for all notations in the following section.

Computation of the arrival time

Because of Snell's law on reflection angles, the geometry presents two isometric triangles. FRR_1 and FEE_1 yield the relation :

$$\frac{b_1}{b_2} = \frac{(Z-Sp)\sin\alpha}{Z\sin\alpha} \qquad that\ is: \qquad b_1 = (1-\frac{Sp}{Z})b_2 \tag{B-1}$$

We also have:

$$b_1 + b_2 = Sp\cos\alpha \tag{B-2}$$

We may solve those two equations for b_1 and b_2, and substitute into the following equations to get a_1 and a_2:

$$a_1^2 = b_1^2 + (Z - Sp)^2\sin^2\alpha \qquad \text{and} \qquad a_2^2 = b_2^2 + Z^2\sin^2\alpha \tag{B-3}$$

After some easy algebra, we end up with:

$$a_1 + a_2 = \sqrt{Sp^2\cos^2\alpha + (2Z - Sp)^2\sin^2\alpha} \tag{B-4}$$

This formula yields the trivial result, $2Z - Sp$ when α is taken to 90^o. We choose to express the result in terms of the nondimensional ratio of the arrival time of the reflected wave, t, over the arrival time of the direct wave, $t_0 = Sp/v_0$ and the ratio of the distance, Z, over the spacing Sp. Let $z = Z/Sp$ vary between 1 and infinity. The final result, then, is:

$$\frac{t}{t_0} = \sqrt{1 + 4z(z - 1)\sin^2\alpha} \tag{B-5}$$

Computation of the apparent velocity of the reflected arrival

Differentiating the two squared terms of the previous equation with respect to t leads to :

$$\frac{1}{2}\frac{t}{t_0^2} = \frac{dz}{dt}(2z - 1)\sin^2\alpha \tag{B-6}$$

Let $d(Sp.z)/dt$ be v_a, the apparent velocity of the reflected wave. We express

this equation in terms of non dimensional ratios as v_α / v_{90}, where v_{90} is the velocity for an horizontal interface, namely, $v_0 / 2$.

$$\frac{v_\alpha}{v_{90}} = \frac{t}{t_0} \frac{1}{(2z - 1)sin^2\alpha} \tag{B-7}$$

Substituting the expression of t / t_0 yields :

$$\frac{v_\alpha}{v_{90}} = \frac{\sqrt{1 + 4z(z - 1)\sin^2\alpha}}{(2z - 1)sin^2\alpha} \tag{B-8}$$

This result is consistent with a velocity of $v_0 / 2$ obtained for a horizontal plane, that is for $\alpha = 90°$. For increasing z, the apparent velocity decreases. We note that for large z, v_α / v_{90} behaves as $1 / \sin\alpha$ and for $z = 1$, it behaves as $1 / \sin^2\alpha$. Figure A-4 presents plots of v_α / v_{90} for $z = 1$, $z = 2$, $z = 3$ and for $z \to \infty$.

APPENDIX C : REFLECTION ON A DIPPING SURFACE WITH CONVERSION.

With the same geometrical configuration as in Appendix B, we shall work out the apparent velocity of a headwave travelling in the formation at velocity v_0 impinging on a plane surface and being reflected with velocity v_1. The apparent velocity of the wave cannot be computed in the same straightforward manner as in Appendix B.

The geometrical problem is very similar to that of Appendix A, except for some sign changes. Following those developments, we first define the reflection point as the intersection of three straight lines analytically defined in a cartesian system of coordinates.

Arrival time

The system is solved, yielding the equation :

$$\tan\alpha \, [\, (Z / Sp) tan\ i + (Z / Sp - 1) tan\ r\,] = 1 \tag{C-1}$$

Snell's law provides us with a second equation, which, together with equation (C-1), defines uniquely the angles and thus the point of reflection.

$$\sin i = V \sin r \tag{C-2}$$

where $V = v_0 / v_1$. In the numerical computations, the angles are worked out by trying successive values until they satisfy both equations (C-1) and (C-2).

Once i and r are known, the arrival time of the reflected event can be ruled out. Let $z = Z / Sp$:

$$\frac{t}{t_0} = \sin\alpha\left[\frac{z}{\cos i} - \frac{(1-z)V}{\cos r}\right] \qquad \text{(C-3)}$$

t_0 is the arrival time of the headwave, refracted in the formation under critical incidence and propagated in the formation with the velocity v_0 directly toward the receiver, that is, under the assumptions made hereby, $t_0 = Sp / v_0$.

Apparent velocity of the reflection arrival

By differentiating both sides of equation (C-3) with respect to z, we obtain an expression for the apparent velocity:

$$\frac{dt}{dz} = t_0 \sin\alpha \left[\frac{1}{\cos i} + \frac{V}{\cos r} + z\frac{\sin i}{\cos^2 i}\frac{di}{dz} - (1-z)V\frac{\sin r}{\cos^2 r}\frac{dr}{dz}\right] \qquad \text{(C-4)}$$

The derivatives of i and r with respect to z can be obtained by solving the linear system resulting from differentiating equations (C-1) and (C-2). Thus we have:

$$\cos r\frac{dr}{dz} = -\frac{\tan r + \tan i}{\frac{(z-1)}{\cos^3 r} + \frac{zV}{\cos^3 i}} \quad \text{and} \quad \cos i\frac{di}{dz} = V\cos r\frac{dr}{dz} \qquad \text{(C-5)}$$

Substituting these two equations in equation (C-4) leads to the final result :

$$\frac{v_{90}}{v_a} = \frac{\sin\alpha}{1+V}[\cos i + V\cos r] \qquad \text{(C-6)}$$

where v_a is the apparent velocity that we have been looking for, and v_{90} the velocity reached for an horizontal reflector, namely, $(v_0^{-1} + v_1^{-1})^{-1}$.

Again, as in Appendix A, problems are to be expected because of the simplifications made to reach result (C-6). A discussion is carried out in the text where two cases are considered. Nevertheless, we escaped the numerical difficulties by computing the apparent velocity at some distance from the interface through an accurate determination of the angles (equations C-1 and C-2). Namely, we took z = 1.1 to generate Figures 7 and 8.

APPENDIX D : SCATTERING POINT IN THE FORMATION

In this model we consider a point in the formation at distance E from the borehole axis. Body waves coming from the transmitter at a velocity v_0 encounter the point and are re-emitted instantaneously with a velocity v_1 toward the receiver. The point acts as a "perfect" scatterer. The algebra is very straightforward.

Arrival time

Let Z be the location of the source; $Z - Sp$ that of the receiver. The distance from the source to the scattering point is $Z^2 + E^2$, while $(Z-Sp)^2 + E^2$ is that from the point to the receiver. Normalizing all the distances with respect to the spacing Sp, and the time with respect to the arrival time of the direct wave at the velocity v_0, we can write:

$$\frac{t}{t_0} = \sqrt{z^2 + e^2} + V\sqrt{(z-1)^2 + e^2} \qquad \text{(D-1)}$$

where $z = Z/Sp$; $e = E/Sp$.

Apparent velocity

As previously, we differentiate the travel time curve to get the apparent velocity, v_a.

$$\frac{v_0}{v_a} = z\left[\frac{1}{\sqrt{z^2 + e^2}} + \frac{V}{\sqrt{(z-1)^2 + e^2}}\right] \qquad \text{(D-2)}$$

We can check that as $z \to \pm\infty$, $v_a^{-1} \to \pm v_0^{-1} + v_1^{-1}$